

**NDACC UV-visible  
total ozone  
measurements**

F. Hendrick et al.

# NDACC UV-visible total ozone measurements: improved retrieval and comparison with correlative satellite and ground-based observations

F. Hendrick<sup>1</sup>, J.-P. Pommereau<sup>2</sup>, F. Goutail<sup>2</sup>, R. D. Evans<sup>3</sup>, D. Ionov<sup>2,4</sup>,  
A. Pazmino<sup>2</sup>, E. Kyrö<sup>5</sup>, G. Held<sup>6</sup>, P. Eriksen<sup>7</sup>, V. Dorokhov<sup>8</sup>, M. Gil<sup>9</sup>, and  
M. Van Roozendaal<sup>1</sup>

<sup>1</sup>Belgian Institute for Space Aeronomy (BIRA-IASB), Brussels, Belgium

<sup>2</sup>LATMOS, CNRS, and University of Versailles Saint Quentin, Guyancourt, France

<sup>3</sup>Earth System Research Laboratory/Global Monitoring Division, National Oceanic and Atmospheric Administration (NOAA), Boulder, Colorado, USA

<sup>4</sup>Department of Atmospheric Physics, Research Institute of Physics, St. Petersburg State University, St. Petersburg, Russia

<sup>5</sup>Arctic Research Center, Finnish Meteorological Institute (FMI), Sodankyla, Finland

<sup>6</sup>Meteorological Research Institute, Universidade Estadual Paulista, Bauru, São Paulo, Brazil

Title Page

Abstract

Introduction

Conclusions

References

Tables

Figures

◀

▶

◀

▶

Back

Close

Full Screen / Esc

Printer-friendly Version

Interactive Discussion



<sup>7</sup>Danish Meteorological Institute, Copenhagen, Denmark

<sup>8</sup>Central Aerological Institute, Dolgoprudny, Russia

<sup>9</sup>Instituto de Tecnica Aeroespacial (INTA), Torrejón de Ardoz, Spain

Received: 16 July 2010 – Accepted: 20 August 2010 – Published: 27 August 2010

Correspondence to: F. Hendrick (franch@oma.be)

Published by Copernicus Publications on behalf of the European Geosciences Union.

**NDACC UV-visible  
total ozone  
measurements**

F. Hendrick et al.

Title Page

Abstract

Introduction

Conclusions

References

Tables

Figures

⏪

⏩

◀

▶

Back

Close

Full Screen / Esc

Printer-friendly Version

Interactive Discussion



## Abstract

Accurate long-term monitoring of total ozone is one of the most important requirements for identifying possible natural or anthropogenic changes in the composition of the stratosphere. For this purpose, the NDACC (Network for the Detection of Atmospheric Composition Change) UV-visible Working Group has made recommendations for improving and homogenizing the retrieval of total ozone columns from twilight zenith-sky visible spectrometers. These instruments, deployed all over the world in about 35 stations, allow measurements of total ozone twice daily with little sensitivity to stratospheric temperature and cloud cover. The NDACC recommendations address both the DOAS retrieval parameters and the calculation of air mass factors (AMF) needed for the conversion of O<sub>3</sub> slant column densities into vertical column amounts. The most important improvement is the use of O<sub>3</sub> AMF look-up tables calculated using the TOMS V8 O<sub>3</sub> profile climatology, that allows accounting for the dependence of the O<sub>3</sub> AMF on the seasonal and latitudinal variations of the O<sub>3</sub> vertical distribution. To investigate their impact on the retrieved ozone columns, the recommendations have been applied to measurements from the NDACC/SAOZ (Système d'Analyse par Observation Zénithale) network. The revised SAOZ ozone data from eight stations covering all latitude regions have been compared to TOMS, GOME-GDP4, SCIAMACHY-TOSOMI, OMI-TOMS, and OMI-DOAS satellite overpass observations, as well as to those of collocated Dobson and Brewer instruments. A significant improvement is obtained after applying the new O<sub>3</sub> AMFs, although systematic seasonal differences between SAOZ and all other instruments remain. These are shown to mainly originate from i) the temperature dependence of the ozone absorption cross sections in the UV being not or improperly corrected by some retrieval algorithms, and ii) the longitudinal differences in tropospheric ozone column being ignored by zonal climatologies. For those measurements sensitive to stratospheric temperature like TOMS, OMI-TOMS, Dobson and Brewer, the application of a temperature correction results in the almost complete removal of the seasonal difference with SAOZ, improving significantly the consistency

### NDACC UV-visible total ozone measurements

F. Hendrick et al.

Title Page

Abstract

Introduction

Conclusions

References

Tables

Figures



Back

Close

Full Screen / Esc

Printer-friendly Version

Interactive Discussion



between all ground-based and satellite total ozone observations.

## 1 Introduction

Started in the UK in the 1930's with the Dobson spectrophotometer, total ozone monitoring now involves a combination of satellite and ground-based observations in the UV, the first with the advantage of global coverage and the last of long-term continuity. However, since the late 1980's, a new ground-based technique making use of zenith-sky UV-visible absorption measurements at twilight has been developed, allowing the monitoring of stratospheric ozone and related trace gases such as NO<sub>2</sub>, BrO, and OCIO (e.g., Pommereau and Goutail, 1988; Solomon et al., 1989; McKenzie, et al., 1991; Kreher et al., 1997; Richter et al., 1999; Van Roozendael et al., 1998). The main difference with the Dobson and Brewer instruments of the Global Atmospheric Watch network of the World Meteorological Organization (GAW/WMO), which are measuring ozone by direct sun and occasionally zenith-sky spectrophotometry in the UV Huggins bands, is the use of the visible Chappuis bands, a wavelength range not applicable to ground-based direct sun or satellite nadir instruments observing at high sun. It enables twice daily O<sub>3</sub> measurements at twilight throughout the year at all latitudes up to the polar circle, with moreover little sensitivity to the cloud cover. In the UV-visible spectrometry technique, trace gas species amounts are retrieved by analyzing zenith-sky radiance spectra at large solar zenith angle (SZA) using the Differential Optical Absorption Spectroscopy (DOAS; Platt and Stutz, 2008) method consisting of fitting the narrow absorption features of the species with laboratory absorption cross sections without further calibration procedure. Slant column densities (SCDs), which are the direct product of the DOAS analysis, are then converted into vertical column densities (VCDs) using the so-called air mass factors (AMFs) derived by radiative transfer calculations from measured or climatological O<sub>3</sub> and atmospheric air density profiles.

### NDACC UV-visible total ozone measurements

F. Hendrick et al.

Title Page

Abstract

Introduction

Conclusions

References

Tables

Figures

◀

▶

◀

▶

Back

Close

Full Screen / Esc

Printer-friendly Version

Interactive Discussion



**NDACC UV-visible  
total ozone  
measurements**

F. Hendrick et al.

Title Page

Abstract

Introduction

Conclusions

References

Tables

Figures

◀

▶

◀

▶

Back

Close

Full Screen / Esc

Printer-friendly Version

Interactive Discussion



The Network for the Detection of Atmospheric Composition Change (NDACC, formerly NDSC), formally operational since 1991, is composed of more than 70 high-quality remote-sensing research stations for observing and understanding the composition and structure of the stratosphere and troposphere. Within NDACC, the UV-visible network consists of more than 35 certified UV-visible spectrometers operating from pole to pole and providing time-series of O<sub>3</sub> and NO<sub>2</sub> total columns made publicly available on the network web site (<http://www.ndacc.org>). These data have been used for the validation of satellite measurements (e.g., Lambert et al., 1999) and trend analysis (e.g., Struthers et al., 2004). Data evaluation and quality assessment procedures, which are under the responsibility of the NDACC UV-visible Working Group (WG), are essential for ensuring the quality of these data sets on a long-term basis. With this objective, the NDACC UV-visible WG is organizing regularly field instruments and algorithms inter-comparison campaigns. The first took place in Lauder (45° S, 170° E) in New Zealand in 1992 (Hofmann et al., 1995), and was followed by several others in Camborne (50° N, 5° W) in the UK in 1994 (Vaughan et al., 1997), at the Observatoire de Haute Provence (OHP; 44° N, 6° E) in France in 1996 (Roscoe et al., 1999), in Andøya (69° N, 16° E) in Norway in 2003 (Vandaele et al., 2005), and in Cabauw (52° N, 5° E) in the Netherlands in 2009 for the CINDI campaign (Roscoe et al., 2010). However, despite this effort of cross evaluations, it has been recognized that the O<sub>3</sub> data sets still suffer from residual inconsistencies mainly due to (1) differences in the DOAS settings, in particular the ozone absorption cross sections used for the various instruments and (2) a lack of homogeneity in the AMFs applied to O<sub>3</sub> slant columns for their conversion into vertical columns. Recently, the NDACC UV-visible WG has formulated recommendations and provided tools and input data sets aiming at improving the homogeneity of the UV-visible total ozone measurements delivered to the NDACC database. Here we report on these recommendations and illustrate the benefit of their use by a comparison between resulting total ozone derived from the French led NDACC/SAOZ (Système d'Analyse par Observation Zénithale) network and collocated observations performed by other instruments.

The present paper is divided into 4 parts. Section 2 provides a description of the NDACC UV-visible WG recommendations for DOAS settings and O<sub>3</sub> AMF calculations. Section 3 is devoted to the analysis of the error budget on the retrieved O<sub>3</sub> vertical columns. An illustration of the application of the recommended settings to the NDACC/SAOZ network is then given in Sect. 4, including a comparison between SAOZ total O<sub>3</sub> columns at different stations from the Arctic to the Antarctic and collocated satellite, Dobson, and Brewer observations. Concluding remarks are given in Sect. 5.

## 2 Total ozone retrieval

Ozone is retrieved in the visible Chappuis bands in a wavelength range of about 100 nm wide centered around 500 nm, taking into account the spectral signature of O<sub>3</sub>, NO<sub>2</sub>, H<sub>2</sub>O, O<sub>4</sub>, and the filling-in of the solar Fraunhofer bands by the Ring effect (Grainger and Ring, 1962).

The O<sub>3</sub> differential slant column density (*DSCD*), which is the amount of O<sub>3</sub> present in the path that the light follows to the instrument minus that from a reference measurement, is the direct product of the DOAS analysis. It is converted into a vertical column amount using the following equation:

$$VCD(\theta) = \frac{DSCD(\theta) + RCD}{AMF(\theta)} \quad (1)$$

where *VCD*( $\theta$ ) is the vertical column density at solar zenith angle (SZA)  $\theta$ , *DSCD*( $\theta$ ) the differential slant column density at SZA  $\theta$ , *RCD* the residual ozone amount in the reference measurement (a fixed spectrum recorded at high sun around local noon), and *AMF*( $\theta$ ) the airmass factor at SZA  $\theta$ .

*RCD* is derived using the so-called Langley plot method, which consists in rearranging Eq. (1) and plotting *DSCD*( $\theta$ ) as a function of *AMF*( $\theta$ ), the intercept at *AMF* = 0 giving *RCD* (Roscoe et al., 1994; Vaughan et al., 1997). Sunrise and sunset O<sub>3</sub> column

Title Page

Abstract

Introduction

Conclusions

References

Tables

Figures

◀

▶

◀

▶

Back

Close

Full Screen / Esc

Printer-friendly Version

Interactive Discussion



data provided to the NDACC database are derived by averaging vertical columns estimated with Eq. (1) over a limited SZA range around  $90^\circ$  SZA (generally  $86\text{--}91^\circ$  SZA). The AMF, also called geometrical enhancement, is defined as the ratio between the slant and vertical column densities (Solomon et al., 1987). It is computed with a radiative transfer model (RTM) initialized with  $\text{O}_3$ , pressure, temperature, and aerosol extinction profiles representative, as much as possible, of the atmosphere at the location of the station. So far, NDACC UV-visible groups commonly used their own RTM calculations (in single or multiple scattering mode) and sets of ozone, pressure and temperature profiles, with or without latitudinal and seasonal variations. Differences between AMFs are causing the largest discrepancies between the NDACC  $\text{O}_3$  data sets. The objective of the recommendations formulated by the NDACC UV-visible WG is the reduction of these discrepancies through the provision of homogeneous tools for calculating appropriate latitude and seasonal dependent AMFs.

## 2.1 Recommended DOAS settings

The NDACC recommendations for the ozone DOAS retrieval are summarized in Table 1. Optimizing retrieval settings for total ozone in the visible Chappuis bands requires consideration on how the differential ozone signal can be extracted with maximum sensitivity, while minimizing spectral interferences with other absorbers, which are, in the present spectral range, water vapor and the collision pair  $\text{O}_2\text{--O}_2$ . From sensitivity studies conducted on simulated spectra and actual measurements, it was found that ozone fitting uncertainties are minimized using the  $450\text{--}550$  nm spectral interval and therefore this one was selected as a baseline for ozone retrieval in the Chappuis bands. Given the importance of wavelength registration for DOAS evaluations in general, the recommendation is that measured spectra are aligned with the highest accuracy. This can be obtained by correlating measured spectra with a reference solar spectrum such as those of Kurucz (1984) or Chance and Spurr (1997), using least-squares techniques as implemented e.g. in the Windoas software suite (Fayt and Van Roozendael, 2001) or in the SAOZ analysis algorithm (Pommereau and Goutail, 1988). Different data sets of

### NDACC UV-visible total ozone measurements

F. Hendrick et al.

Title Page

Abstract

Introduction

Conclusions

References

Tables

Figures



Back

Close

Full Screen / Esc

Printer-friendly Version

Interactive Discussion



ozone absorption cross sections are available from the literature. Comparison studies (e.g. Orphal, 2003) showed that differences of up to 4 percent can occur in the region of the Chappuis bands, and even more in the Huggins bands. Therefore we strongly recommend the use of a common ozone cross section data set to avoid systematic differences. From test evaluations, the data set of Bogumil et al. (2003) is recommended since it gives the smallest variance in the residuals as well as good consistency with the ozone retrieval in the UV Huggins bands. Recommendations for laboratory cross section data sets of other species interfering in the 450–550 nm region are provided in Table 1. Vandaele et al. (1997) at 220° K is generally used for stratospheric NO<sub>2</sub> retrievals and therefore adequate for NO<sub>2</sub> removal in the O<sub>3</sub> fitting range. For correction of the Ring effect filling-in solar Fraunhofer lines, the approach published in Chance and Spurr (1997) is well suited. Note that the ozone differential absorption features are broad enough in the Chappuis bands to ensure that their filling-in by the Ring effect is quite small. However, due to its impact on the Fraunhofer lines, the Ring effect cannot be neglected. As already mentioned, the NDACC recommendation for twilight reporting is to average all available measurements between 86° and 91° SZA. This range minimizes errors due to slant column fitting and AMF calculation (see Sect. 3) and provides measurements of stratospheric ozone with little sensitivity to tropospheric ozone and clouds.

## 2.2 Recommended O<sub>3</sub> AMFs

### 2.2.1 Description

Look-up tables (LUTs) of O<sub>3</sub> AMFs have been developed at the Belgian Institute for Space Aeronomy (BIRA-IASB) in support of the NDACC UV-visible WG. These are based on the TOMS version 8 (TV8) ozone and temperature profile climatology (Bhartia et al., 2004; McPeters et al., 2007). TV8 is a monthly climatology for 10° latitude bands between 90° S and 90° N, covering altitudes from 0 to 60 km, and including a total O<sub>3</sub> column dependence (225–325 Dobson Unit (DU) in the tropics, 225–575 DU at

## NDACC UV-visible total ozone measurements

F. Hendrick et al.

Title Page

Abstract

Introduction

Conclusions

References

Tables

Figures

◀

▶

◀

▶

Back

Close

Full Screen / Esc

Printer-friendly Version

Interactive Discussion



mid-latitudes, and 125–575 DU at high-latitudes, with a 50 DU step). It was built by combining profile data from SAGE II (Stratospheric Aerosol and Gas Experiment II), MLS (Microwave Limb Sounder), and ozonesondes. This climatology has been widely utilized for the retrieval of global total ozone fields from recent US and European UV-visible nadir satellite sounders (e.g., Bhartia et al., 2004; Coldewey-Egbers et al., 2005; Van Roozendaal et al., 2006; Eskes et al., 2005).

The O<sub>3</sub> AMF LUTs are calculated for the eighteen TV8 latitude bands using the UVSPEC/DISORT RTM (Mayer and Kylling, 2005) which is based on the Discrete Ordinate Method and includes a treatment of the multiple scattering in a pseudo-spherical geometry. The model has been validated through several intercomparison exercises (e.g., Hendrick et al., 2006; Wagner et al., 2007). The parameters and their corresponding values used to initialize UVSPEC/DISORT for the calculation of the AMF LUTs are summarized in Table 2. Since the TV8 climatology is limited to the 0–60 km altitude range, the O<sub>3</sub>, temperature, and pressure profiles are complemented above 60 km by the AFGL Standard Atmosphere for matching with the altitude grid chosen in UVSPEC/DISORT for the present study which is 0–90 km. The surface albedo and altitude output values (varying from 0 to 1 and 0 to 4 km, respectively) allow covering all NDACC stations. Regarding the aerosol settings, an aerosol extinction profile corresponding to a background loading has been selected from the aerosol model of Shettle (1989) included in UVSPEC/DISORT. The present O<sub>3</sub> AMF LUTs are thus not suitable in case of large volcanic eruption such as that of the Pinatubo in 1991.

The calculated LUTs depend on the following set of parameters: latitude, day of year, O<sub>3</sub> column, wavelength, SZA, surface albedo, and altitude. An interpolation routine has been designed for extracting appropriately parameterized O<sub>3</sub> AMFs for the various NDACC stations. A global monthly climatology of the surface albedo derived from satellite data at 494 nm (Koelemeijer et al., 2003) is coupled to the interpolation routine, so the latter can be initialized with realistic albedo values in a transparent way. The interpolation routine, O<sub>3</sub> AMF LUTs, albedo climatology as well as DOAS settings are publicly available at <http://uv-vis.aeronomie.be/groundbased>.

**NDACC UV-visible  
total ozone  
measurements**

F. Hendrick et al.

Title Page

Abstract

Introduction

Conclusions

References

Tables

Figures

◀

▶

◀

▶

Back

Close

Full Screen / Esc

Printer-friendly Version

Interactive Discussion



## 2.2.2 Comparison to SAOZ O<sub>3</sub> AMFs

In order to illustrate the impact of using the O<sub>3</sub> AMF LUTs instead of the tropical and mid- and high-latitude SAOZ AMF values, time-series of AMFs have been extracted from the LUTs for one year of data at five stations of the NDACC/ SAOZ network: 5 Sodankyla (67° N, 27° E), Jungfrauoch (47° N, 8° E), Observatoire de Haute Provence (44° N, 6° E), Bauru (22° S, 46°W), and Dumont d'Urville (67° S, 140° E). The wavelength is fixed to 500 nm, surface albedo to 0.2, and altitude output to 0 km, except for Jungfrauoch (altitude: 3.6 km). The O<sub>3</sub> column values needed to properly extract AMFs from the LUTs have been taken from existing measurement data files available 10 from the NDACC database for year 2005. These AMFs have been compared to the SAOZ AMFs calculated for tropical and high- and mid-latitude conditions using annual mean composite O<sub>3</sub> profiles from SAGE II, POAM III, and SAOZ balloon observations. Comparison results are presented in Fig. 1. At mid- and high-latitudes in the Northern Hemisphere, the largest difference is obtained in winter with LUT AMFs larger than the SAOZ ones by up to 8%. In summer, the difference is in the 0–2% range at Sodankyla and OHP but can reach 4% at Jungfrauoch, with LUT AMFs larger than the SAOZ 15 ones, except at Sodankyla. At Dumont d'Urville (high-latitude in the Southern Hemisphere), the LUT AMFs are larger than the SAOZ one with a difference of about 11% in summer and 5% in winter. In the tropics, the LUT AMFs are systematically larger 20 than the SAOZ AMF by up to 5%, with no seasonality in the difference.

## 3 Error budget

### 3.1 DOAS analysis

Systematic uncertainties on the DOAS retrieval are directly related to uncertainties on absorption cross sections. In the current state of knowledge about the ozone spec- 25 troscopy, one can estimate that the absolute accuracy of the ozone cross sections

## NDACC UV-visible total ozone measurements

F. Hendrick et al.

Title Page

Abstract

Introduction

Conclusions

References

Tables

Figures

◀

▶

◀

▶

Back

Close

Full Screen / Esc

Printer-friendly Version

Interactive Discussion



in the Chappuis bands is not better than 2 percent (Orphal, 2003). Beyond this issue, DOAS-type retrievals can be biased for a number of reasons, including spectral interferences with overlapping absorbers and possible instrumental effects such as polarization. It is among the duties of the NDACC UV-visible WG to ensure that the design of participating instruments is sound and properly controlled. This is obtained through adequate intercomparison exercises. Spectral interference effects that may occur in multi-species DOAS fits are more difficult to track and moreover retrieval codes might react differently to them. In order to quantify possible differences between the retrievals, a theoretical exercise has been performed involving simulations of zenith-sky twilight radiances at 89° SZA based on the SCIATRAN v. 2.2 radiative transfer model (Rozanov et al., 2005). Spectra of known ozone slant column amounts were distributed for processing to three independent retrieval teams, each of them using their own retrieval codes configured with the NDACC recommendations. Simulations included different levels of ozone, and O<sub>2</sub>-O<sub>2</sub> absorptions, and the impact of the Ring effect was considered as well. As can be seen in Fig. 2, the three groups were able to derive ozone columns within one percent of the true value for most simulations. Similarly, O<sub>3</sub> retrievals performed by the same teams using a common set of zenith-sky measurements lead to the same level of agreement (results not shown here), from which we can conclude that upon suitable synchronization of retrieval settings, ozone slant columns can be retrieved to within one percent of precision.

### 3.2 AMF LUTs

A potential source of uncertainty in our O<sub>3</sub> AMF calculation is related to the use of the TV8 O<sub>3</sub> profile climatology, which has been originally designed for space nadir backscatter measurements. In order to test the validity of this climatology in the present context, O<sub>3</sub> AMFs extracted from the LUTs have been compared to calculations performed using O<sub>3</sub> profiles measured with O<sub>3</sub> sonde and/or Lidar observations at a set of NDACC stations representative of a wide range of conditions (tropics, mid- and high-latitudes). The stations and the corresponding observations are listed

## NDACC UV-visible total ozone measurements

F. Hendrick et al.

Title Page

Abstract

Introduction

Conclusions

References

Tables

Figures



Back

Close

Full Screen / Esc

Printer-friendly Version

Interactive Discussion



**NDACC UV-visible  
total ozone  
measurements**

F. Hendrick et al.

Title Page

Abstract

Introduction

Conclusions

References

Tables

Figures

◀

▶

◀

▶

Back

Close

Full Screen / Esc

Printer-friendly Version

Interactive Discussion



in Table 3. Measurement data have been downloaded from the NDACC database (<http://www.ndacc.org>). It should be noted that Lidar profiles have been complemented below their covered altitude range by the TV8 climatology. Pressure and temperature profiles are taken from the AFGL Standard Atmosphere when not available in the Lidar measurements data files. The aerosol extinction profile is the same as the one used for the calculation of the LUTs (see Sect. 2.2.1). The other settings needed to initialize the UVSPEC/DISORT RTM are identical to those fixed for the extraction of the  $O_3$  AMFs from the LUTs (wavelength: 500 nm, surface albedo: 0.2, altitude of the station: 0 km).  $O_3$  AMFs are calculated for the  $86\text{--}91^\circ/\text{step } 1^\circ$  SZA range using the measured  $O_3$  profiles and compared to those extracted from the LUTs for the same SZA range. Figure 3 depicts the comparison of calculated and extracted AMFs averaged over the  $86\text{--}91^\circ$  SZA range (these AMFs are called hereafter  $AMF_{86\text{--}91^\circ\text{SZA}}$ ). In average, the largest relative difference between  $O_3$   $AMF_{86\text{--}91^\circ\text{SZA}}$  extracted from the LUTs and those calculated with the measured  $O_3$  profiles is of  $-1.7\%$  (obtained for the Andoya/Lidar case; see also Table 3). The mean relative difference for the nine comparison cases considered here is of  $-1 \pm 1.3\%$ . At some stations (Ny-Ålesund, Izaña, Dumont D'Urville), the difference presents residual seasonalities which could be partly related to the fact that the zonal dependence of the tropospheric ozone seasonality is not implemented in the TV8 climatology. Nevertheless, these comparison results show that the TV8 climatology reproduces well the latitudinal and seasonal variations of the observed  $O_3$  profiles, so that accurate  $O_3$  AMFs can be calculated.

The choice of the aerosol extinction profile is also a source of uncertainty in our  $O_3$  AMF calculation. The UVSPEC/DISORT RTM includes the aerosol climatology of Shettle (1989), which consists of a set of extinction profiles corresponding to different volcanic conditions (background, moderate, high, and extreme). For the present study, we have selected the aerosol extinction profile corresponding to background conditions, with a surface visibility of 40 km (named hereafter the standard settings). In order to give an upper limit for the uncertainty related to the choice of these aerosol settings, sensitivity tests corresponding to moderate volcanic conditions have been performed.

**NDACC UV-visible  
total ozone  
measurements**

F. Hendrick et al.

Title Page

Abstract

Introduction

Conclusions

References

Tables

Figures

◀

▶

◀

▶

Back

Close

Full Screen / Esc

Printer-friendly Version

Interactive Discussion



The  $O_3$  profiles are selected from the TV8 climatology for the following conditions:  $25^\circ N/275$  DU,  $45^\circ N/352$  DU, and  $65^\circ N/325$  DU in June. Figure 4 (upper plots) shows the comparison of  $O_3$  AMFs calculated with standard and moderate volcanic aerosol settings. The relative difference is smaller than 2% except at SZA larger than  $87^\circ$  in the tropics where the  $O_3$  AMFs corresponding to moderate volcanic conditions are larger than the standard ones by up to 4%. However, the mean relative difference in the  $86$ – $91^\circ$  SZA range for the three selected  $O_3$  profiles is of 0.6%. Similar comparison results are obtained for winter  $O_3$  profiles.

The impact of clouds on  $O_3$  AMFs has also been investigated using the water clouds model included in UVSPEC/DISORT. The way to initialize this model is to specify the vertical profile of liquid water content and effective droplet radius. The microphysical properties of water clouds are then converted to optical properties according to the Hu and Stamnes (1993) parameterization.  $O_3$  AMFs are calculated for cloudy and non-cloudy conditions for the same TV8 climatology  $O_3$  profiles as above ( $25^\circ N/275$  DU,  $45^\circ N/352$  DU, and  $65^\circ N/325$  DU in June). For cloudy conditions, the cloud model parameters values are fixed as follows: water content:  $0.3 \text{ g/m}^3$ , effective droplet radius:  $5 \mu\text{m}$ , cloud layer thickness and altitude: 1 km between 1 and 2 km. Since these parameters values correspond to a rather large stratus cloud (Shettle, 1989), the present sensitivity test gives us an upper limit for the impact of clouds on  $O_3$  AMFs. A comparison of  $O_3$  AMFs calculated for cloudy and non-cloudy conditions is presented in Fig. 4 (middle plots). Cloudy AMFs are systematically larger than non-cloudy AMFs by about 5–8% at  $86^\circ$  SZA and 2% at  $91^\circ$  SZA. The mean relative difference in the  $86$ – $91^\circ$  SZA range for the three selected  $O_3$  profiles is of 3.3%. Similar comparison results are obtained for winter  $O_3$  profiles. It should be noted that the corresponding impact of clouds on  $O_4$  AMFs is about 70%. Therefore, such cloudy events can be easily identified and filtered out using simultaneous  $O_4$  measurements obtained from the same instrument.

Another source of uncertainty investigated in this study is related to the choice of RTM. Although previous studies (e.g., Hendrick et al., 2006; Wagner et al., 2007) have demonstrated that, for AMF calculation, the UVSPEC/DISORT model shows very good

consistency with others RTMs, a verification exercise has been carried out to firmly assess the reliability of  $O_3$  AMF calculations. It consists in comparing  $O_3$  AMFs calculated using the UVSPEC/DISORT and SCIATRAN v2.2 RTMs initialized in the same way. SCIATRAN is based on the Combining Differential-Integral approach using the Picard-Iterative approximation (CDIPI) and includes a treatment of multiple scattering in full or pseudo-spherical geometry (Rozanov et al., 2005). The following settings have been used for the present exercise: geometry: pseudo-spherical, TV8  $O_3$  profile climatology, AFGL Standard Atmosphere pressure and temperature profiles, TV8 atmosphere layering (Umkehr layers), wavelength: 541 nm, surface albedo: 0, altitude of the station: 0 km. Regarding the  $O_3$  profile, the following cases have been considered: polar in January and June ( $65^\circ$  N and S with a total column of 325 DU, mid-latitude in January and June ( $45^\circ$  N and S, 325 DU), and tropics in January and June ( $25^\circ$  N and S, 275 DU). The results for the Northern Hemisphere in June are shown in Fig. 4 (lower plots). Both models are in excellent agreement with relative differences smaller than 1.5%. In the  $86\text{--}91^\circ$  SZA range, the mean relative difference is 0.7%. Since similar consistency is found in January and in the Southern Hemisphere, this comparison demonstrates the reliability of the UVSPEC/DISORT RTM for  $O_3$  AMF calculation.

In addition, the influence of the ozone profile climatology used in the  $O_3$  AMF LUT calculations has been also investigated by comparing AMFs derived using SCIATRAN with the TV8, the University of Bremen atmospheric model for trace gases, and the Fortuin and Kelder (1998) climatologies. Differences (not shown here) were very small, indicating that the choice of climatology has little impact on AMF calculations.

The overall error budget on twilight zenith-sky visible retrievals of  $O_3$  total columns is summarized in Table 4. The total error of 4.6% is estimated by adding in quadrature the different sources of uncertainty investigated here.

**NDACC UV-visible  
total ozone  
measurements**

F. Hendrick et al.

Title Page

Abstract

Introduction

Conclusions

References

Tables

Figures

◀

▶

◀

▶

Back

Close

Full Screen / Esc

Printer-friendly Version

Interactive Discussion



## 4 Application to the NDACC/SAOZ network

The French led SAOZ (Système d'Analyse par Observation Zénithale) network contributes significantly to the NDACC/UV-visible network with about 20 instruments covering a wide range of latitudes in both hemispheres (see Table 5). The SAOZ instrument is a broad-band (300-600 nm), medium resolution (1 nm) diode-array spectrometer that measures the sunlight scattered from the zenith sky (Pommereau and Goutail, 1988; Sarkissian et al., 1997). Absorption spectra are recorded every hour at solar zenith angle (SZA) smaller than 85° and every 5 minutes during twilight up to 94° SZA. For evaluating the change in the SAOZ performances when applying the NDACC recommendations, the full data set has been reprocessed in a version V2 (the previous version is called V1 here below). The V2 data set is compared to satellite overpass observations and collocated ground-based Dobson and Brewer measurements.

### 4.1 Comparison to satellite observations

Five total ozone satellite data series are available since the beginning of the deployment of the SAOZ network in 1988: the TOMS V8 series from Nimbus-7, Meteor-3, and Earth Probe between 1989 and 2005 available from the NASA GSFC database (<http://toms.gsfc.nasa.gov>, Wellemeyer et al., 1999); the GOME-GDP4 observations from 1995 to 2003 for all stations and until present for the European sector after the failure of the onboard data recorder, available from the operational ESA GDP4 level 2 (<http://wdc.dlr.de/sensors.gome/gdp4/>; Van Roozendaal et al., 2006); the SCIAMACHY-TOSOMI columns since 2002, available from the ESA - KNMI TEMIS site ([http://www.temis.nl/protocols/o3col/overpass\\_scia.html](http://www.temis.nl/protocols/o3col/overpass_scia.html); Eskes et al., 2005), the AURA OMI-TOMS and OMI-DOAS collection 3 retrievals since 2004 available at the NASA AVDC (<http://avdc.gsfc.nasa.gov>; Veeffkind et al., 2006; Kroon et al., 2008). All the data used here are overpass total ozone columns above each station within a 300 km radius. Eight SAOZ stations have been selected for the present comparison (see details in Table 5): three in the Arctic (Scoresbysund, Zhigansk, and Sodankyla), one at

## NDACC UV-visible total ozone measurements

F. Hendrick et al.

Title Page

Abstract

Introduction

Conclusions

References

Tables

Figures



Back

Close

Full Screen / Esc

Printer-friendly Version

Interactive Discussion



northern mid-latitude (Observatoire de Haute Provence), two at the southern tropics (Reunion Island and Bauru), one at the southern mid-latitude (Kerguelen) and one in the Antarctic (Dumont d'Urville). Because of the perturbation of the SAOZ zenith-sky total ozone measurements by the volcanic aerosols injected in the stratosphere by the eruption of Mount Pinatubo in 1991, the measurements performed between October 1991 and October 1992 have been ignored.

#### 4.1.1 V2 versus V1 SAOZ data sets

As an example, monthly mean total ozone column and relative difference satellite-SAOZ V2 at OHP since 1995 for TOMS and GOME-GDP4 (the two longest satellite records) are presented in Fig. 5. The difference shows a systematic seasonal variation with a summer maximum. The amplitude of the seasonal cycle of the difference is larger with TOMS (4.7%) than with GOME-GDP4 (1.2%).

Figure 6 depicts the change between V1 and V2 SAOZ data sets of the seasonal cycle of the difference satellite-SAOZ at Sodankyla, OHP, Bauru and Dumont d'Urville. The use of V2 instead of V1 reduces the amplitude of the seasonal cycle of the difference with TOMS from 10.8% to 6.3% at Sodankyla and from 8.0% to 4.7% at OHP and from 11.0% to 8.3% and 4.9% to 1.2% for the same stations with GOME-GDP4. SAOZ V2 has little impact at Bauru (tropics), where the amplitude of the relative difference varies from 1.8% to 1.5% with TOMS and from 3.5% to 3.0% with GOME-GDP4. The comparison in the Antarctic is only slightly improved, with still a significant seasonal cycle with a strong spring maximum.

Table 6 summarizes the change in the seasonal cycle of the satellite-SAOZ difference for all selected stations and satellites. On average, the replacement of the SAOZ V1 data set by the version V2 reduces the amplitude of the seasonal cycle, but partly only (a systematic seasonal cycle of large amplitude can remain in some cases). Since the relative difference satellite-SAOZ always shows frequently a maximum in summer out of phase with the total ozone seasonal cycle (maximum in spring, minimum in fall), it must be attributed to something else. Potential parameters, known to show a

### NDACC UV-visible total ozone measurements

F. Hendrick et al.

Title Page

Abstract

Introduction

Conclusions

References

Tables

Figures

◀

▶

◀

▶

Back

Close

Full Screen / Esc

Printer-friendly Version

Interactive Discussion



similar seasonal cycle are the temperature of the stratosphere, -and possibly also the contribution of tropospheric ozone.

#### 4.1.2 Stratospheric temperature dependence

The stratospheric temperature dependence has been investigated by correlating the satellite-SAOZ difference with daily ECMWF temperature at 50 hPa and 30 hPa which display a mean seasonal cycle with a maximum of amplitude in summer increasing with latitude from 10–12 K in the tropics, 15–20 K at mid-latitude, 30–35 K in the Arctic and 50 K in the Antarctic. The correlation was performed on daily measurements from all stations together (sunrise-sunset average in case of SAOZ). For removing systematic mean differences between the stations discussed in Sect. 4.1.3, the average bias of each station is normalized to zero at 210 K. As an example, Fig. 7 shows the correlation at 50 hPa for TOMS and GOME-GDP4 involving more than 30 000 data points after removing the satellite measurements at  $SZA > 84^\circ$  at high latitude where they are known as less reliable. The resulting slopes and standard deviation at 50 and 30 hPa for all satellites are presented in Table 7. Since the 50 hPa level corresponds to the altitude of the maximum ozone concentration in polar region where the amplitude of the temperature seasonal cycle is the largest, the results are very similar for the two levels though the slopes at 30 hPa are on average slightly smaller. TOMS shows the largest positive dependence, followed by OMI-TOMS, while GOME-GDP4 has less sensitivity and SCIAMACHY-TOSOMI and OMI-DOAS a negative dependence. Since SAOZ measures in the visible Chappuis band where the ozone absorption cross sections are known to have very little dependence with temperature (Voigt et al., 2001; Brion et al., 2004), the difference satellite-SAOZ reveals a temperature dependence of the absorption cross sections in the UV, known to exist but likely not properly quantified or accounted for in the satellite retrievals.

Figure 8 shows the residual seasonal variation of the satellite – SAOZ V2 relative difference in the Arctic, northern mid-latitude, tropics and Antarctic for all satellites after correction for the temperature dependence as summarised in Table 7. The residual

### NDACC UV-visible total ozone measurements

F. Hendrick et al.

Title Page

Abstract

Introduction

Conclusions

References

Tables

Figures

◀

▶

◀

▶

Back

Close

Full Screen / Esc

Printer-friendly Version

Interactive Discussion



## NDACC UV-visible total ozone measurements

F. Hendrick et al.

Title Page

Abstract

Introduction

Conclusions

References

Tables

Figures

⏪

⏩

◀

▶

Back

Close

Full Screen / Esc

Printer-friendly Version

Interactive Discussion



seasonal amplitudes before and after applying the correction are presented in Table 8. With most of the satellites, the amplitude of the difference decreases, particularly at high latitude and for the most temperature sensitive satellite measurements like those from TOMS. However, systematic seasonal variations remain, often showing a summer maximum but not always, particularly with GOME-GDP4, SCIAMACHY-TOSOMI and OMI-DOAS which are displaying a maximum difference in spring at high latitude where the total ozone is the largest. Since these features are not present with all satellites, they can hardly be attributed to the SAOZ retrievals. There may be several explanations for that, e.g. an imperfect correction for temperature dependence of the ozone absorption cross sections, but also possible limitations in other aspects of the satellite retrievals. Satellite retrievals indeed have largest uncertainties in the polar region for a number of reasons. First, backscattered UV measurements are sensitive to surface albedo, which can be highly variable especially at the edge of the polar cap. Moreover, current satellite algorithms cannot distinguish clouds from underlying bright surfaces, and therefore the impact of clouds on total ozone retrievals remains highly uncertain in snow/ice conditions. In particular the treatment of the ozone partial column hidden beneath thick clouds (the so-called ozone ghost-column) is not well controlled and might lead to systematic errors in current satellite data products. Another possible source of uncertainty is related to the large variability of the ozone concentration field, especially in spring conditions at the edge of the polar vortex. This variability in space and time might not be appropriately captured by the ozone profile climatology used for both satellite and SAOZ retrievals despite the adopted ozone column classification.

### 4.1.3 Biases and precision

More insight into the possible origin of the above differences is provided by an examination of the statistics of the comparison for each station. Figure 9 shows the bias and the dispersion of the satellite-SAOZ V2 difference for all stations and satellites (see also Table 9 for corresponding values). On average (bottom line of Table 9), the total ozone derived by the satellites is 0.8% larger than that of SAOZ, that is within the 1%

absolute accuracy of the absorption cross sections in the visible (Bogumil et al., 2003). However, there are systematic deviations between satellite families, which cannot thus be attributed to SAOZ. At high latitude and particularly in the Antarctic, SCIAMACHY-TOSOMI, GOME-GDP4 and OMI-DOAS are overestimating the total ozone compared to TOMS, OMI-TOMS and SAOZ and in addition the two first are showing a larger dispersion. Note that the impact is particularly large at Dumont d'Urville on the East Antarctic most frequently outside the vortex in spring where large ozone columns (350–400 DU) are reported, with vertical profile shapes totally different from those observed in the ozone hole over the West Antarctic. These results are consistent with the maximum difference between GOME-GDP4, SCIAMACHY-TOSOMI, OMI-DOAS and SAOZ at high latitude in spring (see Fig. 8) although no clear explanation was found for that.

Another remarkable feature in Fig. 9, is the jump seen by all satellites between the two tropical stations of Reunion Island and Bauru (see also Table 9), where the stratospheric ozone column is the same since the TV8 climatology is zonal and the two stations are at the same latitude. A first explanation is that this could originate from an error in the amount of ozone remaining in the SAOZ reference spectrum. But tests showed that this error could not account for more than 0.3%. Another potential explanation is the influence of tropospheric ozone, known to be larger over the Indian Ocean than over Southern Brazil (Thompson et al., 2003; see also Table 10), to which SAOZ is little sensitive compared to nadir viewing satellites because of the amplification of the stratospheric contribution by about a factor of 15 in the twilight zenith-sky observing geometry.

## 4.2 Tropospheric ozone contribution

Because of the smaller stratospheric column, the relative contribution of tropospheric ozone (TOZ) to the total column is larger in the tropics, where it reaches 30–40 DU, which corresponds to 10–15% of the total column. A well known feature of tropical TOZ, is wave number one longitudinal distribution with a maximum over Africa and the Indian Ocean (Thompson et al., 2003), ignored in a zonal profile climatology. Figure 10

### NDACC UV-visible total ozone measurements

F. Hendrick et al.

Title Page

Abstract

Introduction

Conclusions

References

Tables

Figures



Back

Close

Full Screen / Esc

Printer-friendly Version

Interactive Discussion



shows the TOZ seasonal cycles over Reunion Island and Bauru derived from weekly ECC sondes for the first and a combination of Mozaic aircraft over Sao Paulo (Marengo et al., 1998; www.cnrm.meteo.fr/mozaic/) and SAGE II (www.sage2.larc.nasa.gov/) measurements over Brazil, and those retrieved by OMI between 0–15 km altitude by subtracting the MLS stratospheric ozone from the OMI column (Ziemke et al., 2006). On average, the tropospheric column is larger by 6–8 DU over Reunion Island. This results in 2–3% larger total column, which is of the same order of magnitude of the difference between satellite total columns over the two stations.

### 4.3 Comparison to Dobson and Brewer

Two ground-based UV ozone spectrophotometers are collocated with SAOZ instruments, a Dobson at OHP and a Brewer at Sodankyla, to which SAOZ measurements have been compared.

#### 4.3.1 Dobson at OHP

The instrument is the Dobson #085 operating at this station since 1983. A comparison of the total ozone columns measured by the Dobson and SAOZ (V2 retrieval) spectrometers is presented in Fig. 11. As for satellite instruments, the difference Dobson-SAOZ shows a systematic seasonal variation with a maximum in summer. The amplitude of this effect is 6.9% with SAOZ V1 while it decreases to 3.2% with SAOZ V2 (see Fig. 12). The correlation with ECMWF temperature indicates a dependence of the difference Dobson-SAOZ V2 of  $0.25 \pm 0.02\% / ^\circ\text{C}$  at 50 hPa and  $0.20 \pm 0.01\% / ^\circ\text{C}$  at 30 hPa, or  $0.18\% / ^\circ\text{C}$  using the NCEP temperature at 30 hPa. The 30 hPa temperature is more relevant at OHP since it corresponds better to the altitude of the maximum of ozone concentration. After correction for the temperature dependence at 50 hPa, the amplitude of the seasonal variation decreases to 1.3% with an average bias of  $-0.8 \pm 3.8\%$ . At 30 hPa, the corresponding values are 1.2% and  $-1.1 \pm 3.7\%$ , respectively. Using the 30 hPa NCEP temperature and the  $0.13\% / ^\circ\text{C}$  dependence (Komhyr et al., 1993)

## NDACC UV-visible total ozone measurements

F. Hendrick et al.

Title Page

Abstract

Introduction

Conclusions

References

Tables

Figures

◀

▶

◀

▶

Back

Close

Full Screen / Esc

Printer-friendly Version

Interactive Discussion



derived from the Bass and Paur ozone cross sections (Paur and Bass, 1985), the amplitude of the seasonal variation is 1.5%, with an average bias of  $-1.3 \pm 3.6\%$ .

The temperature dependence derived by the above correlations is significantly larger than the  $0.13\%/^{\circ}\text{C}$  for the Dobson AD pair calculated by Komhyr et al. (1993), the  $0.11\%/^{\circ}\text{C}$  proposed by Van Roozendaal et al. (1998) from the cross sections of Malicet et al. (1995), and the  $0.02\%/^{\circ}\text{C}$  from Burrows et al. (1999), as summarized by Scarnato et al. (2009). Aside from an error in the absorption cross sections, a possible additional contribution to the seasonal variation of the difference with SAOZ could be the influence of tropospheric ozone to which, in contrast to Dobson direct sun observations, SAOZ is little sensitive. As shown in Fig. 13, the tropospheric ozone column at OHP has a systematic seasonality of about 15 DU amplitude with a maximum in summer, in phase with the temperature cycle. It is slightly larger than the 10 DU amplitude derived from the TOMS V8 zonal climatology. This could lead to an additional seasonal cycle of 1-1.5% amplitude in the Dobson-SAOZ difference, on top of a systematic bias due to the average overestimation of climatological tropospheric column by 10 DU (see Fig. 13).

The Dobson instrument has internal stray light that produces an error with a SZA dependence and which is more pronounced at high ozone values. The magnitude of the error is difficult to estimate, but can contribute to the seasonal cycle of the Dobson-SAOZ differences, as the largest amplitude is in late winter-early spring at OHP.

In summary, the 3.2% apparent seasonal amplitude of difference Dobson-SAOZ V2 could be largely explained by the temperature dependence of the absorption cross sections not corrected for in the Dobson measurements, the seasonal variation of the tropospheric column to which SAOZ is little sensitive, and internal stray light in the Dobson instrument, although an underestimation of the temperature sensitivity of the Dobson AD pair cannot be ruled-out.

### 4.3.2 Brewer MKII at Sodankyla

The Brewer and the SAOZ instruments in Sodankyla were already compared in 1990–1991 (Kyrö, 1993). The SAOZ showed a systematic bias varying from  $-9 \pm 5\%$  if only

## NDACC UV-visible total ozone measurements

F. Hendrick et al.

Title Page

Abstract

Introduction

Conclusions

References

Tables

Figures

◀

▶

◀

▶

Back

Close

Full Screen / Esc

Printer-friendly Version

Interactive Discussion



Brewer measurements at SZA  $<60^\circ$  were considered and +2% using all Brewer data. The seasonal cycle of the ratio between the Brewer and SAOZ measurements were highly correlated with the temperature at 50 hPa, but at a rate of  $0.34\%/^\circ\text{C}$ , exceeding largely the  $0.07\%/^\circ\text{C}$  Brewer temperature dependence derived by Kerr et al. (1988) from the  $\text{O}_3$  cross sections of Paur and Bass (1985). At that time, no explanation was found for this discrepancy but the SAOZ retrieval was the V1 version based on the use of a constant AMF derived from a mean winter ozone profile. Figure 14 shows the Brewer and SAOZ V2 series of ozone column over Sodankyla since 1990 and the corresponding relative difference. A systematic seasonal cycle of 3–4% amplitude is found, with a significant drop during the winter month where only the Brewer zenith-sky measurements are available. This seasonal cycle, limited to the Brewer direct sun measurements, is depicted in Fig. 15. The change from SAOZ V1 to SAOZ V2 decreases the amplitude of the seasonal cycle from 6.5 to 2.4%, providing an explanation to the Kyrö (1993) interrogation. The correlation with ECMWF temperature indicates a dependence of the Brewer -SAOZ difference of  $0.09\pm 0.01\%/^\circ\text{C}$  at 50hPa and of  $0.08\pm 0.01\%/^\circ\text{C}$  at 30 hPa, the first being most relevant at this latitude. After correction for the temperature dependence at 50 hPa, the amplitude of the seasonal variation decreases to 1.5% with an average bias of  $1.9\pm 3.2\%$  (the corresponding values at 30hPa are 1.3% and  $1.9\pm 3.2\%$ ), with no sign of a summer maximum. Though larger than the 0.07% initially estimated by Kerr et al. (1988), the temperature dependence of  $0.09\pm 0.01\%/^\circ\text{C}$  provided by the present correlation is fully consistent with the estimates of  $0.11\%/^\circ\text{C}$  of Van Roozendael et al. (1998) or the  $0.09\%/^\circ\text{C}$  of Kerr et al. (2002) from the same Paur and Bass (1985) cross sections but using different sets of temperature (Scarnato et al., 2009).

Savastiouk and McElroy (2010) have estimated that a change from Paur and Bass (1985) to Malicet et al. (1995) absorption cross sections would make the Brewer data lower by a factor of 0.97 in average. This would bring Sodankyla SAOZ and Brewer data in even better agreement. It should be also mentioned that single Brewer like Dobson instruments suffer from stray light problems during high ozone slant path conditions

**NDACC UV-visible  
total ozone  
measurements**

F. Hendrick et al.

Title Page

Abstract

Introduction

Conclusions

References

Tables

Figures

◀

▶

◀

▶

Back

Close

Full Screen / Esc

Printer-friendly Version

Interactive Discussion



(Scarnato et al., 2009), typically in March to early April at Sodankyla but it has little effect on the overall comparison.

## 5 Conclusions

The NDACC UV-visible Working Group has made recommendations on the spectral analysis settings and AMF calculation for the retrieval of total ozone columns from ground-based zenith-sky UV-visible observations. The aim of these recommendations is to improve the homogeneity of the visible total ozone measurements delivered to the NDACC database. The main change, compared to the settings utilized so far, is the use of O<sub>3</sub> AMF LUTs based on the TOMS V8 O<sub>3</sub> profile climatology, which allows accounting for the dependence of the O<sub>3</sub> AMF on the latitudinal and seasonal variations of the ozone vertical profile. The calculated LUTs, which are suitable only for an aerosol loading corresponding to background conditions, depend on latitude, day of year, O<sub>3</sub> column, wavelength, SZA, surface albedo, and altitude of the station. The main sources of uncertainty in our O<sub>3</sub> AMF calculation have been identified as the use of an O<sub>3</sub> profile climatology instead of observational data, the choice of the aerosol extinction profile and the RTM, as well as the presence or absence of clouds. Taking into account these uncertainties, the total error on the O<sub>3</sub> AMFs has been estimated to be 3.5%, which combined with uncertainties on slant column retrievals lead to a total uncertainty of 4.6%.

For evaluating the change in the SAOZ performances when applying the NDACC recommendations, the full SAOZ data set has been reprocessed and compared to satellite overpass observations from the TOMS, GOME-GDP4, SCIAMACHY-TOSOMI, OMI-TOMS, and OMI-DOAS data products for a selection of eight stations, as well as to collocated ground-based Dobson and Brewer measurements at OHP and Sodankyla, respectively. Regarding the comparison with satellites, the agreement is significantly improved when using the new SAOZ data set (called version V2). However, some systematic seasonal variation in the difference satellite–SAOZ V2 remains, largely origi-

### NDACC UV-visible total ozone measurements

F. Hendrick et al.

Title Page

Abstract

Introduction

Conclusions

References

Tables

Figures

◀

▶

◀

▶

Back

Close

Full Screen / Esc

Printer-friendly Version

Interactive Discussion



## NDACC UV-visible total ozone measurements

F. Hendrick et al.

Title Page

Abstract

Introduction

Conclusions

References

Tables

Figures

⏪

⏩

◀

▶

Back

Close

Full Screen / Esc

Printer-friendly Version

Interactive Discussion



5 nating from a stratospheric temperature dependence which is particularly large on the short UV TOMS and OMI-TOMS retrievals. Since the visible Chappuis bands used by SAOZ are little sensitive to temperature, it is very likely coming from errors in ozone absorption cross sections in the UV or inadequate correction for temperature dependence. After correcting for temperature, the amplitude of the seasonal variation of the satellite-SAOZ differences decreases significantly, particularly with TOMS and OMI-TOMS. The average bias of all satellites with SAOZ is less than 1% with a standard deviation of  $\pm 2\%$ , except for SCIAMACHY-TOSOMI and OMI-TOMS for which it increases up to  $\pm 3.5\text{--}4\%$ . However, even after temperature correction, systematic seasonal features still remain at all latitudes, but with larger amplitude in polar regions, especially in the Antarctic with GOME-GDP4, SCIAMACHY-TOSOMI and OMI-DOAS. They are tentatively attributed (1) to longitudinal changes of tropospheric ozone ignored when using mean zonal profile climatology and to which the SAOZ zenith sky measurements at twilight are little sensitive in contrast to nadir viewing satellites, and (2) to limitations in current satellite retrievals for the high latitudes. After applying the LUT AMF on SAOZ and correcting the satellites for the temperature dependences, the amplitude of the seasonal difference between satellites and SAOZ decreases to less than 2% at mid-latitude and in the tropics and to 5–7% in polar regions.

20 The use of the  $O_3$  AMF LUTs reduces also the difference between Dobson, Brewer, and SAOZ total ozone measurements. But, as for satellites, systematic seasonal variations of the difference with SAOZ still remain, originating in the temperature dependence of the ozone absorption cross sections in the UV and possibly also in the local seasonal cycle of tropospheric ozone partly represented in the zonal profile climatology used for calculating the  $O_3$  AMF LUTs. When corrected for the temperature dependence, the average difference with daily SAOZ total ozone columns is reduced to  $-0.8\pm 3.8\%$  and  $1.9\pm 3.2\%$  for the Dobson and Brewer instruments, respectively.

25 Overall, the application of the NDACC UV-visible Working Group recommendations, together with the correction for the temperature dependence of UV ground-based and satellite observations, leads to a significantly improved consistency of total ozone long-

term series, allowing more accurate identification of possible natural or anthropogenic changes in the composition of the stratosphere.

*Acknowledgements.* The authors thank the many SAOZ, Brewer and Dobson operators in stations without whom the long series of data used in this paper would not have been available as well as agencies supporting NDACC activities: INSU/CNRS, CNES, IPEV. This work was supported by the ESA Multi-Taste, EC GEOMon, and Belgian PRODEX SECPEA projects. The authors are also thankful to the PIs of the Lidar and ECC sondes O<sub>3</sub> profile data used in this study and downloaded from the NDACC database: P. von der Gathen (AWI), G. Hansen and K. Stebel (NILU), S. Godin-Beekmann, G. Ancellet, and F. Goutail (LATMOS/CNRS), A. Redondas (INME-IZO), F. Posny (Université de la Réunion), G. Bodeker (NIWA), and D. Swart (RIVM). N. Theys (BIRA-IASB) is acknowledged for calculating time-series of tropopause height at various NDACC stations.

## References

- Bhartia, P. K., Wellemeyer, C. G., Taylor, S. L., Nath, N., and Gopalan, A.: Solar Backscatter (SBUV) Version 8 profile algorithm, in: Proceedings of the Quadrennial Ozone Symposium 2004, Athens, Greece, edited by C. Zerefos, ISBN 960-630-103-6, 295–296, 2004.
- Bogumil, K., Orphal, J., Homann, T., Voigt, S., Spietz, P., Fleischmann, O. C., Vogel, A., Hartmann, M., Bovensmann, H., Frerik, J., and Burrows, J. P.: Measurements of molecular absorption spectra with the SCIAMACHY Pre-Flight Model: Instrument characterization and reference spectra for atmospheric remote sensing in the 230-2380 nm region, *J. Photochem. Photobiol. A*, 157, 167–184, 2003.
- Brion, J., Chakir, A., Charbonnier, J., Daumont, D., Parisse, C., and Malicet, J.: Absorption Spectra Measurements for the Ozone Molecule in the 350–830 nm Region, *J. Atm. Chem.*, 30, 291–299, doi:10.1023/A:1006036924364, 2004.
- Burrows, J. P., Richter, A., Dehn, A., Deters, B., Himmelmann, S., Voigt, S., and Orphal, J.: Atmospheric Remote-sensing reference data from GOME – 2. Temperature-dependent absorption cross sections of O<sub>3</sub> in the 231-794 nm range, *J. Quant. Spectrosc. Radiat. Transfer*, 61(4), 509–517, 1999.
- Chance, K. and Spurr, R. J. D.: Ring effect studies: Rayleigh scattering including molecular

## NDACC UV-visible total ozone measurements

F. Hendrick et al.

Title Page

Abstract

Introduction

Conclusions

References

Tables

Figures

◀

▶

◀

▶

Back

Close

Full Screen / Esc

Printer-friendly Version

Interactive Discussion



**NDACC UV-visible  
total ozone  
measurements**

F. Hendrick et al.

Title Page

Abstract

Introduction

Conclusions

References

Tables

Figures

◀

▶

◀

▶

Back

Close

Full Screen / Esc

Printer-friendly Version

Interactive Discussion



parameters for rotational Raman scattering, and the Fraunhofer spectrum, Appl. Opt., 36, 5224–5230, 1997.

Coldewey-Egbers, M., Weber, M., Lamsal, L. N., de Beek, R., Buchwitz, M., and Burrows, J. P.: Total ozone retrieval from GOME UV spectral data using the weighting function DOAS approach, Atmos. Chem. Phys., 5, 1015–1025, doi:10.5194/acp-5-1015-2005, 2005.

Eskes, H. J., van der A, R. J., Brinksma, E. J., Veefkind, J. P., de Haan, J. F., and Valks, P. J. M.: Retrieval and validation of ozone columns derived from measurements of SCIAMACHY on Envisat, Atmos. Chem. Phys. Discuss., 5, 4429–4475, doi:10.5194/acpd-5-4429-2005, 2005.

Fayt, C. and Van Roozendael, M.: WinDOAS 2.1 Software User Manual, available online at: <http://uv-vis.aeronomie.be/software>, 2001.

Fortuin, J. P. F. and Kelder, H.: An ozone climatology based on ozone sondes and satellite measurements, J. Geophys. Res., 103, 31709–31734, 1998.

Grainger, J. and Ring, J.: Anomalous Fraunhofer line profiles, Nature, 193, p. 762, 1962.

Hendrick, F., Van Roozendael, M., Kylling, A., Petritoli, A., Sanghavi, S., Schofield, R., von Friedeburg, C., Wittrock, F., and De Mazière, M.: Intercomparison exercise between different radiative transfer models used for the interpretation of ground-based zenith-sky and multi-axis DOAS observations, Atmos. Chem. Phys., 6, 93–108, doi:10.5194/acp-6-93-2006, 2006.

Hofmann, D., Bonasoni, P., De Mazière, M., Evangelisti, F., Sarkissian, A., Giovanelli, G., Goldman, A., Goutail, F., Harder, J., Jakoubek, R., Johnston, P., Kerr, J., McElroy, T., McKenzie, R., Mount, G., Pommereau, J.-P., Simon, P., Solomon, S., Stutz, J., Thomas, A., Van Roozendael, M., and Wu, E.: Intercomparison of UV/visible spectrometers for measurements of stratospheric NO<sub>2</sub> for the Network for the Detection of Stratospheric Change, J. Geophys. Res., 100, 16765–16791, 1995.

Hu, Y. X. and Stamnes, K.: An accurate parameterization of the radiative properties of water clouds suitable for use in climate models, J. Climate, 6, 728–742, 1993.

Keim, C., Eremenko, M., Orphal, J., Dufour, G., Flaud, J.-M., Höpfner, M., Boynard, A., Clerbaux, C., Payan, S., Coheur, P.-F., Hurtmans, D., Claude, H., Dier, H., Johnson, B., Kelder, H., Kivi, R., Koide, T., López Bartolomé, M., Lambkin, K., Moore, D., Schmidlin, F. J., and Stübi, R.: Tropospheric ozone from IASI: comparison of different inversion algorithms and validation with ozone sondes in the northern middle latitudes, Atmos. Chem. Phys., 9, 9329–9347, doi:10.5194/acp-9-9329-2009, 2009.

**NDACC UV-visible  
total ozone  
measurements**

F. Hendrick et al.

Title Page

Abstract

Introduction

Conclusions

References

Tables

Figures

◀

▶

◀

▶

Back

Close

Full Screen / Esc

Printer-friendly Version

Interactive Discussion



Kerr, J. B., McElroy, C. T., Wardle, D. I., Olafson, R. A., and Evans, W. F. J.: The automated Brewer spectrophotometer, in: Proceedings of the Quadrennial Ozone Symposium 1984, Halkidiki, Greece, edited by: Zerefos, C. S. and Ghazi, A., 396–401, 1984.

5 Koелеmeijer, R. B. A., de Haan, J. F., and Stammes, P.: A database of spectral surface reflectivity in the range 335–772 nm derived from 5.5 years of GOME observations, *J. Geophys. Res.*, 108(D2), 4070, doi:10.1029/2002JD002429, 2003.

Komhyr, W.D, Mateer, C. L., and Hudson, R. D.: Effective Bass and Paur 1985 ozone absorption coefficients for the use with Dobson ozone spectrophotometers, *J. Geophys. Res.*, 98, 20451–20465, 1993.

10 Kreher, K., Johnston, P. V., Wood, S. W., and Platt, U.: Ground-based measurements of tropospheric and stratospheric BrO at Arrival Heights (78° S), Antarctica, *Geophys. Res. Lett.*, 24, 3021–3024, 1997.

Kroon, M., Veefkind, J. P., Sneep, M., McPeters, R. D., Bhartia, P. K., and Levelt, P. F.: Comparing OMI-TOMS and OMI-DOAS total ozone column data, *J. Geophys. Res.*, 113, D16S28, doi:10.1029/2007JD008798, 2008.

15 Kyrö, E.: Intercomparison of total ozone data from Nimbus-7 Toms, the Brewer UV spectrophotometer and SAOZ UV-Visible spectrometer at high latitudes observatory, Sodankyla, *Geophys. Res. Lett.* 20, 571–574, 1993.

Lambert, J.-C., Van Roozendael, M., De Mazière, M., Simon, P. C., Pommereau, J.-P., Goutail, F., Sarkissian, A., and Gleason, J. F.: Investigation of pole-to-pole performances of spaceborne atmospheric chemistry sensors with the NDSC, *J. Atmos. Sci.*, 56, 176–193, 1999.

20 Malicet, J., Daumont, D., Charbonnier, J., Parisse, C., Chakir, A., and Brion, J.: Ozone UV spectroscopy. II. Absorption cross sections and temperature dependence, *J. Atm. Chem.*, 21, 263–273, 1995.

25 Marengo, A., Thouret, V., Nédélec, P., Smit, H., Helten, M., Kley, D., Karcher, F., Simon, P., Law, K., Pyle, J., Poschmann, G., Von Wrede, R., Hume, C., and Cook, T.: Measurement of ozone and water vapor by Airbus in-service aircraft: The MOZAIC airborne program-An overview, *J. Geophys. Res.*, 103, 25631–25642, 1998.

Mayer, B. and Kylling, A.: Technical note: The LibRadtran software package for radiative transfer calculations – Description and examples of use, *Atmos. Chem. Phys.*, 5, 1855–1877, doi:10.5194/acp-5-1855-2005, 2005.

30 McKenzie, R. L., Johnston, P. V., McElroy, C. T., Kerr, J. B., and Solomon, S.: Altitude distributions of stratospheric constituents from ground-based measurements at twilight, *J. Geophys.*

**NDACC UV-visible  
total ozone  
measurements**

F. Hendrick et al.

Title Page

Abstract

Introduction

Conclusions

References

Tables

Figures

◀

▶

◀

▶

Back

Close

Full Screen / Esc

Printer-friendly Version

Interactive Discussion



Res., 96, 15499–15512, 1991.

McPeters, R. D., Labow, G. J., and Logan, J. A.: Ozone climatological profiles for satellite retrieval algorithms, *J. Geophys. Res.*, 112, D05308, doi:10.1029/2005JD006823, 2007.

Orphal, J.: A critical review of the absorption cross sections of O<sub>3</sub> and NO<sub>2</sub> in the 240–790 nm region, *J. Photochem. Photobiol. A: Chem.*, 157, 185–209, 2003.

Paur, R. J. and Bass, A. M.: The ultraviolet cross sections of ozone, II, Result and temperature dependence, in: *Atmospheric Ozone*, C. Zerefos and A. Ghazi (eds), D. Reidel, Dordrecht, The Netherlands, 611–616, 1985.

Platt, U. and Stutz, J.: *Differential Optical Absorption Spectroscopy (DOAS), Principles and Applications*, ISBN 978-3-540-21193-8, Springer, Berlin-Heidelberg, Germany, 2008.

Pommereau, J.-P. and Goutail, F.: O<sub>3</sub> and NO<sub>2</sub> ground-based measurements by visible spectrometry during arctic winter and spring 1988, *Geophys. Res. Lett.*, 15, 891–894, 1988.

Richter, A., Eisinger, M., Ladstätter Weißenmayer, A., Wittrock, F., and Burrows, J. P.: DOAS zenith-sky observations: 2. Seasonal variations of BrO over Bremen (53° N) 1994–1995, *J. Atmos. Chem.*, 32, 83–99, 1999.

Roscoe, H. K., Squires, J. A. C., Oldham, D. J., Sarkissian, A., Pommereau, J.-P., and Goutail, F.: Improvements to the accuracy of zenith-sky measurements of total ozone by visible spectrometers, *J. Quant. Spectrosc. Radiat. Transfer*, 52(5), 639–648, 1994.

Roscoe, H. K., Johnston, P. V., Van Roozendaal, M., Richter, A., Sarkissian, A., Roscoe, J., Preston, K. E., Lambert, J.-C., Hermans, C., Decuyper, W., Dzienus, S., Winterrath, T., Burrows, J. P., Goutail, F., Pommereau, J.-P., D’Almeida, E., Hottier, J., Coureul, C., Didier, R., Pundt, I., Bartlett, L. M., McElroy, C. T., Kerr, J. E., Elokhov, A., Giovanelli, G., Ravegnani, F., Premuda, M., Kostadinov, I., Erle, F., Wagner, T., Pfeilsticker, K., Kenntner, M., Marquard, L. C., Gil, M., Puentedura, O., Yela, M., Arlander, D. W., Kastad Hoiskar, B. A., Tellefsen, C. W., Karlsen Tørnkvist, K., Heese, B., Jones, R. L., Aliwell, S. R., and Freshwater, R. A.: Slant column measurements of O<sub>3</sub> and NO<sub>2</sub> during the NDSC intercomparison of zenith-sky UV-visible spectrometers in June 1996, *J. Atmos. Chem.*, 32, 281–314, 1999.

Roscoe, H. K., Van Roozendaal, M., Fayt, C., du Piesanie, A., Abuhassan, N., Adams, C., Akrami, M., Cede, A., Chong, J., Clmer, K., Friess, U., Gil Ojeda, M., Goutail, F., Graves, R., Griesfeller, A., Grossmann, K., Hemerijckx, G., Hendrick, F., Herman, J., Hermans, C., Irie, H., Johnston, P. V., Kanaya, Y., Kreher, K., Leigh, R., Merlaud, A., Mount, G. H., Navarro, M., Oetjen, H., Pazmino, A., Perez-Camacho, M., Peters, E., Pinardi, G., Puentedura, O., Richter, A., Schnhardt, A., Shaiganfar, R., Spinei, E., Strong, K., Takashima, H., Vlemmix,

**NDACC UV-visible  
total ozone  
measurements**

F. Hendrick et al.

Title Page

Abstract

Introduction

Conclusions

References

Tables

Figures

◀

▶

◀

▶

Back

Close

Full Screen / Esc

Printer-friendly Version

Interactive Discussion



T., Vrekoussis, M., Wagner, T., Wittrock, F., Yela, M., Yilmaz, S., Boersma, F., Hains, J., Kroon, M., and Peters, A.: Intercomparison of slant column measurements of NO<sub>2</sub> and O<sub>4</sub> by MAX-DOAS and zenith-sky UV and visible spectrometers, *Atmos. Meas. Tech. Discuss.*, 3, 3383–3423, doi:10.5194/amtd-3-3383-2010, 2010.

5 Rothman, L. S., Jacquemart, D., Barbe, A., Chris Benner, D., Birk, M., Brown, L. R., Carleer, M. R., Chackerian Jr. C., Chance, K., Coudert, L. H., Dana, V., Devi, V. M., Gamache, R. R., Goldman, A., Jucks, K. W., Maki, A. G., Massie, S. T., Orphal, J., Perrin, A., Rinsland, C. P., Smith, M. A. H., Tennyson, J., Tolchenov, R. N., Toth, R. A., Vander Auwera, J., Varanasi, P., and Wagner, G.: The Hitran 2004 molecular spectroscopic database, *J. Quant. Spectrosc. Radiat. Transfer*, 96, 139–204, 2005.

10 Rozanov, A., Rozanov, V., Buchwitz, M., Kokhanovsky, A., and Burrows, J. P.: SCIATRAN 2.0. A new radiative transfer model for geophysical applications in the 175–2400 nm spectral region, *Adv. Space Res.*, 36(5), 1015–1019, 2005.

15 Sarkissian, A., Vaughan, G., Roscoe, H. K., Bartlett, L. M., O'Connor, F. M., Drew, D. G., Hughes, P. A., and Moore, D. M.: Accuracy of measurements of total ozone by a SAOZ ground-based zenith-sky visible spectrometer, *J. Geophys. Res.*, 102(D1), 1379–1390, 1997.

20 Savastiouk, V. and McElroy, T.: The effect of change of BP to DBM ozone absorption cross sections on total ozone from Brewer, ICAGO Ozone Theme Meeting, Geneva, Switzerland, 23–25 March 2010, [http://igaco-o3.fmi.fi/ACSO/presentations\\_2010/ground-based/OTM\\_2010\\_Savastiouk.pdf](http://igaco-o3.fmi.fi/ACSO/presentations_2010/ground-based/OTM_2010_Savastiouk.pdf).

Scarnato, B., Staehelin, J., Peter, T., Gröbner, J., and Stübi, R.: Temperature and slant path effects in Dobson and Brewer total ozone measurements, *J. Geophys. Res.*, 114, D24303, doi:10.1029/2009JD012349, 2009.

25 Shettle, E. P.: Models of aerosols, clouds, and precipitation for atmospheric propagation studies, in: NATO AGARD Conference Proceedings No. 454: Atmospheric propagation in the UV, visible, IR and mm-region and related system aspects, Neuilly sur Seine, France, 1989.

Solomon, S., Schmeltekopf, A. L., and Sanders, R. W.: On the interpretation of zenith-sky absorption measurements, *J. Geophys. Res.*, 92, 8311–8319, 1987.

30 Solomon, S., Sanders, R. W., Carroll, M. A., and Schmeltekopf, A. L.: Visible and near-ultraviolet spectroscopy at McMurdo station, Antarctica, 5. Diurnal variation of OClO and BrO, *J. Geophys. Res.*, 94, 11393–11403, 1989.

Struthers, H., Kreher, K., Austin, J., Schofield, R., Bodeker, G., Johnston, P., Shiona, H., and

**NDACC UV-visible  
total ozone  
measurements**

F. Hendrick et al.

Title Page

Abstract

Introduction

Conclusions

References

Tables

Figures

◀

▶

◀

▶

Back

Close

Full Screen / Esc

Printer-friendly Version

Interactive Discussion



Thomas, A.: Past and future simulations of NO<sub>2</sub> from a coupled chemistry-climate model in comparison with observations, *Atmos. Chem. Phys.*, 4, 2227–2239, doi:10.5194/acp-4-2227-2004, 2004.

Thompson, A. M., Witte, J. C., Oltmans, S. J., Schmidlin, F. J., Logan, J. A., Fujiwara, M., Kirchhoff, V. W. J. H., Posny, F., Coetzee, G. J. R., Hoegger, B., Kawakami, S., Ogawa, T., Fortuin, J. P. F., and Kelder, H. M.: Southern Hemisphere Additional Ozonesondes (SHADOZ) 1998–2000 tropical ozone climatology 2. Tropospheric variability and the zonal wave-one, *J. Geophys. Res.*, 108(D2), 8241, doi:10.1029/2002JD002241, 2003.

Vandaele, A. C., Hermans, C., Simon, P. C., Carleer, M., Colin, R., Fally, S., Mérieu, M.-F., Jenouvrier, A., and Coquart, B.: Measurements of the NO<sub>2</sub> absorption cross section from 42000 cm<sup>-1</sup> to 10000 cm<sup>-1</sup> (238–1000 nm) at 220 K and 294 K, *J. Quant. Spectrosc. Radiat. Transfer*, 59, 171–184, 1997.

Vandaele, A. C., Fayt, C., Hendrick, F., Hermans, C., Humbled, F., Van Roozendael, M., Gil, M., Navarro, M., Puentedura, O., Yela, M., Braathen, G., Stebel, K., Tørnkvist, K., Johnston, P., Kreher, K., Goutail, F., Mieville, A., Pommereau, J.-P., Khaikine, S., Richter, A., Oetjen, H., Wittrock, F., Bugarski, S., Frieß, U., Pfeilsticker, K., Sinreich, R., Wagner, T., Corlett, G., and Leigh, R.: An intercomparison campaign of ground-based UV-Visible measurements of NO<sub>2</sub>, BrO, and OClO slant columns. Methods of analysis and results for NO<sub>2</sub>, *J. Geophys. Res.*, 110, D08305, doi:10.1029/2004JD005423, 2005.

Van Roozendael, M., Peters, P., Roscoe, H. K., De Backer, H., Jones, A. E., Bartlett, L., Vaughan, G., Goutail, F., Pommereau, J.-P., Kyrö, E., Wahlstrom, C., Braathen, G., and Simon, P. C.: Validation of ground-based visible measurements of total ozone by comparison with Dobson and Brewer spectrophotometers, *J. Atm. Chem.*, 29, 55–83, 1998.

Van Roozendael, M., Loyola, D., Spurr, R., Balis, D., Lambert, J.-C., Livschitz, Y., Valks, P., Ruppert, T., Kenter, P., Fayt, C., and Zehner, C.: Ten years of GOME/ERS-2 total ozone data—The new GOME data Processor (GDP) version 4: 1 Algorithm description, *J. Geophys. Res.* 111, D14311, doi:10.1029/2005JD006375, 2006.

Vaughan, G., Roscoe, H. K., Bartlett, L. M., O'Connor, F., Sarkissian, A., Van Roozendael, M., Lambert, J.-C., Simon, P. C., Karlsen, K., Kaestad Hoiskar, B. A., Fish, D. J., Jones, R. L., Freshwater, R., Pommereau, J.-P., Goutail, F., Andersen, S. B., Drew, D. G., Hughes, P. A., Moore, D., Mellqvist, J., Hegels, E., Klupfel, T., Erle, F., Pfeilsticker, K., and Platt, U.: An intercomparison of ground-based UV-visible sensors of ozone and NO<sub>2</sub>, *J. Geophys. Res.*, 102, 1411–1422, 1997.

**NDACC UV-visible  
total ozone  
measurements**

F. Hendrick et al.

[Title Page](#)[Abstract](#)[Introduction](#)[Conclusions](#)[References](#)[Tables](#)[Figures](#)[⏪](#)[⏩](#)[◀](#)[▶](#)[Back](#)[Close](#)[Full Screen / Esc](#)[Printer-friendly Version](#)[Interactive Discussion](#)

- Veefkind, J. P., de Haan, J. F., Brinksma, E. J., Kroon, M., and Levelt, P. F.: Total ozone from the Ozone Monitoring Instrument (OMI) using the OMI DOAS technique, *IEEE Trans. Geo. Remote Sens.*, 44(5), 1239–1244, 2006.
- Voigt, S., Orphal, J., Bogumil, K., and Burrows, J. P.: The temperature dependence (203-293 K) of the absorption cross sections of O<sub>3</sub> in the 230-850 nm region measured by Fourier-transform spectroscopy, *J. Photochem. Photobiol. A*, 143, 1–9, 2001.
- Wagner, T., Burrows, J. P., Deutschmann, T., Dix, B., von Friedeburg, C., Frieß, U., Hendrick, F., Heue, K.-P., Irie, H., Iwabuchi, H., Kanaya, Y., Keller, J., Mc Linden, C. A., Oetjen, H., Palazzi, E., Petritoli, A., Platt, U., Postlyakov, O., Pukite, J., Richter, A., Van Roozendaal, M., Rozanov, A., Sinreich, R., Sanghavi, S., and Wittrock, F.: Comparison of box-air-mass-factors and radiances for multiple-axis differential optical absorption spectroscopy (MAX-DOAS) geometries calculated from different UV/visible radiative transfer models, *Atmos. Chem. Phys.*, 7, 1809–1833, doi:10.5194/acp-7-1809-2007, 2007.
- Wellemeier, C. G., Bhartia, P. K., Taylor, S. L., Qin, W., and Ahn, C., Version 8 Total Ozone Mapping Spectrometer (TOMS) Algorithm, in: *Proceedings of the Quadrennial Ozone Symposium 2004*, Athens, Greece, edited by C. Zerefos, ISBN 960-630-103-6, 635–636, 2004.
- Ziemke, J. R., Chandra, S., Duncan, B. N., Froidevaux, L., Bhartia, P. K., Levelt, P. F., and Waters, J. W.: Tropospheric ozone determined from Aura OMI and MLS: Evaluation of measurements and comparison with the Global Modeling Initiative's Chemical Transport Model, *J. Geophys. Res.*, 111, D19303, doi:10.1029/2006JD007089, 2006.

## NDACC UV-visible total ozone measurements

F. Hendrick et al.

Title Page

Abstract

Introduction

Conclusions

References

Tables

Figures

◀

▶

◀

▶

Back

Close

Full Screen / Esc

Printer-friendly Version

Interactive Discussion



**Table 1.** Settings recommended for the UV-visible retrieval of O<sub>3</sub> vertical columns.

Parameter	Recommendation
Fitting interval	450–550 nm
Wavelength calibration	Calibration based on reference solar atlas
Cross sections	
O <sub>3</sub>	Bogumil et al. (2003), 223° K
NO <sub>2</sub>	Vandaele et al. (1997), 220° K
H <sub>2</sub> O	Hitran 2004 (Rothman et al., 2005)
O <sub>4</sub>	Hermans ( <a href="http://spectrolab.aeronomie.be/o2.htm">http://spectrolab.aeronomie.be/o2.htm</a> )
Ring effect	NDACC source for Ring effect correction
Molecular and aerosol scattering	Polynomial of order 3, or equivalent non-polynomial high-pass filtering
AMF calculation	BIRA-IASB O <sub>3</sub> AMF LUTs
Determination of residual amount in reference spectrum	Langley plot (Vaughan et al., 1997)
SZA range for twilight averaging of vertical columns	86–91° SZA

## NDACC UV-visible total ozone measurements

F. Hendrick et al.

Title Page

Abstract

Introduction

Conclusions

References

Tables

Figures

◀

▶

◀

▶

Back

Close

Full Screen / Esc

Printer-friendly Version

Interactive Discussion



**Table 2.** Parameters used to initialize the UVSPEC/DISORT RTM for the calculation of the O<sub>3</sub> AMF LUTs.

Parameter	Value
O <sub>3</sub> profile	TV8: <ul style="list-style-type: none"> <li>– Latitude: 85° S to 85° N step 10°</li> <li>– Month: 1 (Jan) to 12 (Dec) step 1</li> <li>– Ozone column: 125 to 575 DU step 50 DU</li> </ul>
Temperature and pressure profiles	TV8
Altitude grid	0 to 120 km step 1 km
Wavelength	440 to 580 nm step 35 nm
Surface albedo	0 and 1
Altitude output	0 and 4 km
SZA	30, 50, 70, 80, 82.5, 85, 86, 87, 88, 89, 90, 91, and 92°

## NDACC UV-visible total ozone measurements

F. Hendrick et al.

Title Page

Abstract

Introduction

Conclusions

References

Tables

Figures

◀

▶

◀

▶

Back

Close

Full Screen / Esc

Printer-friendly Version

Interactive Discussion



**Table 3.** List of O<sub>3</sub> profile measurements used for testing the validity of the TV8 climatology for O<sub>3</sub> AMF calculation. The last column is the mean relative difference (and the corresponding 1σ standard deviation) between O<sub>3</sub> AMF<sub>86–91°SZA</sub> extracted from the LUTs and calculated using the O<sub>3</sub> profiles measured at the different NDACC stations (see Fig. 3).

Station	Instrument	Time period	Number of profiles	Mean O <sub>3</sub> AMF <sub>86–91°SZA</sub> difference (%)
Ny-Ålesund (79° N, 12° E)	O <sub>3</sub> sonde	01/2004–12/2006	218	−0.3±1.3
Andoya (69° N, 16° E)	Lidar	01/2004–12/2006	122	−1.7±1.1
OHP (44° N, 6° E)	O <sub>3</sub> sonde	01/2003–12/2006	113	−1.1±1.3
	Lidar	01/2004–12/2006	377	−1.2±0.7
Izaña (28° N, 16° W)	O <sub>3</sub> sonde	01/2004–12/2006	218	0.5±1.7
Reunion Island (21° S, 55° E)	O <sub>3</sub> sonde	01/2000–12/2002	59	−0.8±1.8
Lauder (45° S, 170° E)	O <sub>3</sub> sonde	01/2004–12/2006	139	−1.3±0.9
	Lidar	01/2004–12/2006	208	−1.4±0.7
Dumont d'Urville (67° S, 140° E)	O <sub>3</sub> sonde	07/2002–12/2006	116	0.4±2.0

## NDACC UV-visible total ozone measurements

F. Hendrick et al.

Title Page

Abstract

Introduction

Conclusions

References

Tables

Figures

◀

▶

◀

▶

Back

Close

Full Screen / Esc

Printer-friendly Version

Interactive Discussion



**Table 4.** Error budget on zenith-sky visible retrievals of total O<sub>3</sub> columns (in %).

Error source	Error on O <sub>3</sub> VCD (%)
Slant column fit	1.0
O <sub>3</sub> cross sections (systematic error)	2.0
O <sub>3</sub> AMF	
TV8 climatology	1
Clouds	3.3
Aerosols	0.6
Albedo	0.2
RTM	0.7
AMF wavelength	1.7
Residual column	0.7
Total	4.6

## NDACC UV-visible total ozone measurements

F. Hendrick et al.

Title Page

Abstract

Introduction

Conclusions

References

Tables

Figures

◀

▶

◀

▶

Back

Close

Full Screen / Esc

Printer-friendly Version

Interactive Discussion



**Table 5.** List of the SAOZ network stations.

Station	Location	Time coverage
Ny-Ålesund (NYA)	78° N, 12° E	1991–
Thule (THU)	76° N, 69° W	1991–
ScoresbySund (SCO)	71° N, 22° W	1991–
Sodankyla (SOD)	67° N, 27° E	1990–
Zhigansk (ZHI)	67° N, 123° E	1992–
Salekhard (SAL)	67° N, 67° E	1998–
Aberyswyth (ABE)	52° N, 4° W	1991–
Jungfrauoch (JFJ)	47° N, 8° E	1990–
Observatoire de Haute Provence (OHP)	44° N, 6° E	1992–
Tarawa (TAR)	1° N, 173° E	1992–1999
Saint-Denis (REU)	21° S, 55° E	1993
Bauru (BAU)	22° S, 49° W	1995
Kerguelen (KER)	49° S, 70° E	1995–
Faraday (FAR)	65° S, 64° W	1990–1996
Rothera (ROT)	67° S, 68° W	1997–
Dumont d'Urville (DDU)	67° S, 140° E	1988–

## NDACC UV-visible total ozone measurements

F. Hendrick et al.

**Table 6.** Amplitude of the seasonal cycle of the relative percent differences satellite – SAOZ (V1/V2). See Table 5 for the meaning of the abbreviations of the stations.

Station	TOMS	GOME-GDP4	SCIAMACHY-TOSOMI	OMI-TOMS	OMI-DOAS
SCO	8.8/4.8	9.8/9.6	9.0/12.0	3.9/2.4	10.7/12.8
ZHI	8.2/4.9	9.3/6.4	9.6/15.3	6.0/8.4	6.7/11.3
SOD	10.8/6.3	11.0/8.3	2.9/6.0	6.3/4.0	3.5/5.6
OHP	8.0/4.7	4.9/1.2	3.0/2.8	7.7/3.4	4.0/2.0
REU	2.1/1.4	4.4/3.4	2.2/1.8	3.1/2.6	1.9/1.8
BAU	1.8/1.5	3.5/3.0	2.5/3.1	3.6/3.0	2.2/2.8
KER	3.9/2.8	1.9/2.0	1.7/3.1	2.2/1.7	2.2/3.7

[Title Page](#)
[Abstract](#)
[Introduction](#)
[Conclusions](#)
[References](#)
[Tables](#)
[Figures](#)
[Back](#)
[Close](#)
[Full Screen / Esc](#)
[Printer-friendly Version](#)
[Interactive Discussion](#)


## NDACC UV-visible total ozone measurements

F. Hendrick et al.

**Table 7.** Temperature dependence of satellite-SAOZ V2 relative difference at 50 and 30 hPa (in %/°C).

Satellite	50 hPa	30 hPa
TOMS	+0.23±0.003	+0.22±0.003
GOME-GDP4	+0.08±0.004	+0.06±0.004
SCIAMACHY-TOSOMI	-0.10±0.007	-0.10±0.007
OMI-TOMS	+0.14±0.004	+0.10±0.004
OMI-DOAS	-0.09±0.006	-0.12±0.006

[Title Page](#)
[Abstract](#)
[Introduction](#)
[Conclusions](#)
[References](#)
[Tables](#)
[Figures](#)
[Back](#)
[Close](#)
[Full Screen / Esc](#)
[Printer-friendly Version](#)
[Interactive Discussion](#)


## NDACC UV-visible total ozone measurements

F. Hendrick et al.

**Table 8.** Residual amplitude of the satellite-SAOZ V2 difference seasonal cycle (in %) before/after temperature correction at 50 hPa. See Table 5 for the meaning of the abbreviations of the stations.

Station	TOMS	GOME-GDP4	SCIAMACHY-TOSOMI	OMI-TOMS	OMI-DOAS
SCO	4.8/5.8	9.6/9.8	12.0/6.4	2.4/3.5	12.8/7.9
ZHI	4.9/1.3	6.4/4.8	15.3/9.9	8.4/6.8	11.3/7.3
SOD	6.3/2.3	8.3/5.9	6.0/3.8	4.0/3.1	5.6/3.1
OHP	4.7/2.7	1.2/1.1	2.8/1.9	3.4/0.9	2.0/1.7
REU	1.4/1.1	3.4/2.1	1.8/1.1	2.6/1.3	1.8/1.4
BAU	1.5/0.9	3.0/2.7	3.1/1.4	3.0/1.8	2.8/1.5
KER	2.8/1.0	2.0/1.2	3.1/2.8	1.7/1.9	3.7/2.4
DDU	10.2/5.6	5.1/6.1	7.0/6.4	7.0/3.2	10.2/4.6

[Title Page](#)
[Abstract](#)
[Introduction](#)
[Conclusions](#)
[References](#)
[Tables](#)
[Figures](#)
[Back](#)
[Close](#)
[Full Screen / Esc](#)
[Printer-friendly Version](#)
[Interactive Discussion](#)




## NDACC UV-visible total ozone measurements

F. Hendrick et al.

Title Page

Abstract

Introduction

Conclusions

References

Tables

Figures

◀

▶

◀

▶

Back

Close

Full Screen / Esc

Printer-friendly Version

Interactive Discussion



**Table 10.** Mean total ozone difference between Reunion and Bauru shown in Fig. 9.

Satellite	Reu-Bau (%)
TOMS	2.6
GOME-GDP4	3.9
SCIAMACHY-TOSOMI	2.7
OMI-TOMS	6.2
OMI-DOAS	3.9

**NDACC UV-visible  
total ozone  
measurements**

F. Hendrick et al.

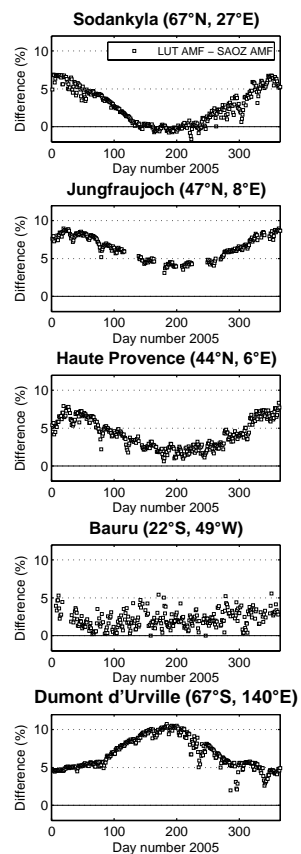


**Fig. 1.** Relative differences between LUT and SAOZ O<sub>3</sub> AMFs at 90° SZA for the year 2005 at Sodankyla (67° N, 27° E), Jungfrauoch (47° N, 8.0° E), Haute Provence (44° N, 6° E), Bauru (22° S, 49° W), and Dumont d'Urville (67° S, 140° E). The SAOZ tropical, high- and mid-latitude O<sub>3</sub> AMF values at 90° SZA are 16.20, 16.22, and 16.52, respectively.

Title Page

Abstract

Introduction

Conclusions

References

Tables

Figures

◀

▶

◀

▶

Back

Close

Full Screen / Esc

Printer-friendly Version

Interactive Discussion



**NDACC UV-visible  
total ozone  
measurements**

F. Hendrick et al.

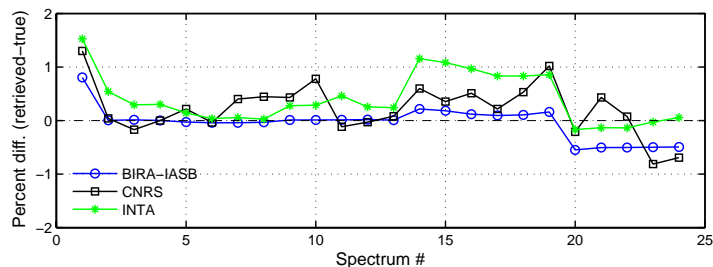


**Fig. 2.** Percent difference between retrieved and true slant column ozone values, as obtained from analysis of simulated radiances independently processed at BIRA-IASB, INTA and LAT-MOS (labeled CNRS in the plot).

[Title Page](#)[Abstract](#)[Introduction](#)[Conclusions](#)[References](#)[Tables](#)[Figures](#)[◀](#)[▶](#)[◀](#)[▶](#)[Back](#)[Close](#)[Full Screen / Esc](#)[Printer-friendly Version](#)[Interactive Discussion](#)

## NDACC UV-visible total ozone measurements

F. Hendrick et al.

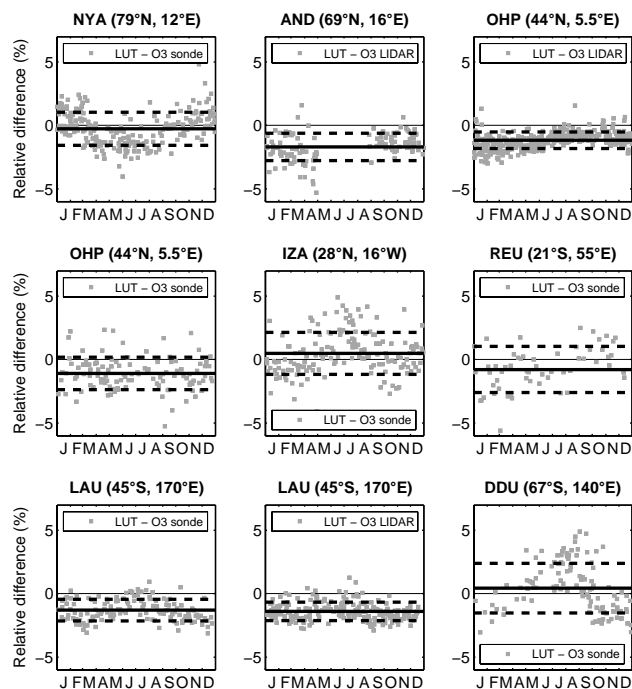


**Fig. 3.** Relative difference between  $O_3$   $AMF_{86-91SZ4}$  extracted from the LUTs and calculated using the  $O_3$  profiles measured at the following NDACC stations: Ny-Ålesund (NYA), Andoya (AND), Observatoire de Haute Provence (OHP), Izaña (IZA), Reunion Island (REU), Lauder (LAU), and Dumont d'Urville (DDU). Grey plain squares: daily relative differences, black solid line: yearly mean relative difference, and black dashed line:  $1\sigma$  standard deviation (see Table 3 for corresponding values).

[Title Page](#)
[Abstract](#)
[Introduction](#)
[Conclusions](#)
[References](#)
[Tables](#)
[Figures](#)
[◀](#)
[▶](#)
[◀](#)
[▶](#)
[Back](#)
[Close](#)
[Full Screen / Esc](#)
[Printer-friendly Version](#)
[Interactive Discussion](#)


## NDACC UV-visible total ozone measurements

F. Hendrick et al.

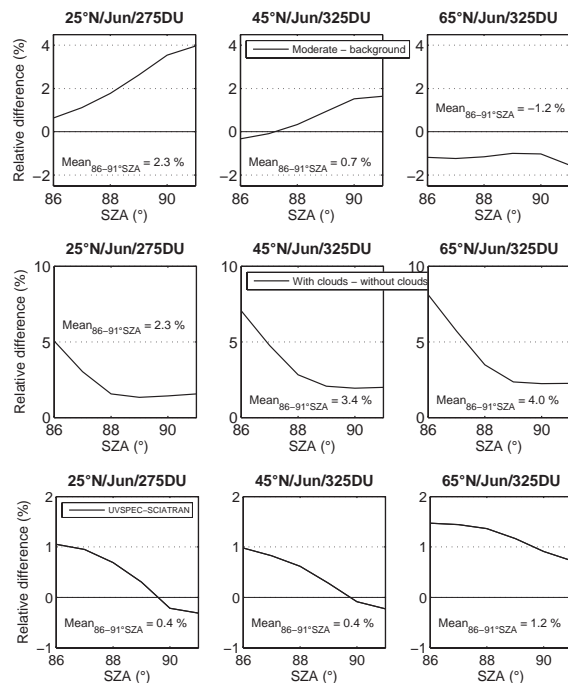


**Fig. 4.** Comparison of  $O_3$  AMFs calculated using standard and moderate volcanic aerosol settings (upper plots), with and without the presence of clouds (middle plots), and with UVSPEC and SCIATRAN RTMs (lower plots). The mean relative difference calculated in the 86–91° SZA range appears on each plot. In case of the aerosols sensitivity test, the overall mean relative difference over the 86–91° SZA range is of 0.6% while it reaches 3.3% for the test on clouds, and 0.7% for the test on RTMs. The  $O_3$  profiles selected from the TV8 climatology for the present comparison correspond to the following conditions: 25° N/275DU (left plots), 45° N/325DU (middle plots), and 65° N/325DU (right plots) in June. The wavelength, surface albedo, and altitude are fixed to 500 nm, 0.2, and 0 km, respectively.

**NDACC UV-visible  
total ozone  
measurements**

F. Hendrick et al.

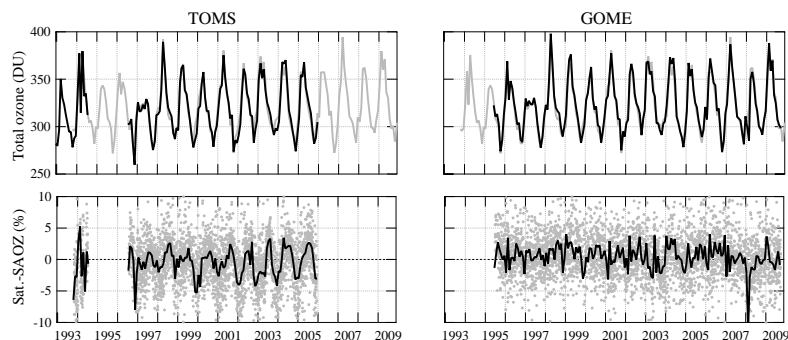


**Fig. 5.** Example of comparison between SAOZ V2 and satellite overpass total ozone at OHP. Top: monthly mean total ozone (SAOZ in grey and satellite in black), bottom: satellite-SAOZ relative difference (grey: daily, black: monthly mean). Left: TOMS, right: GOME-GDP4.

Title Page

Abstract

Introduction

Conclusions

References

Tables

Figures

◀

▶

◀

▶

Back

Close

Full Screen / Esc

Printer-friendly Version

Interactive Discussion



**NDACC UV-visible  
total ozone  
measurements**

F. Hendrick et al.

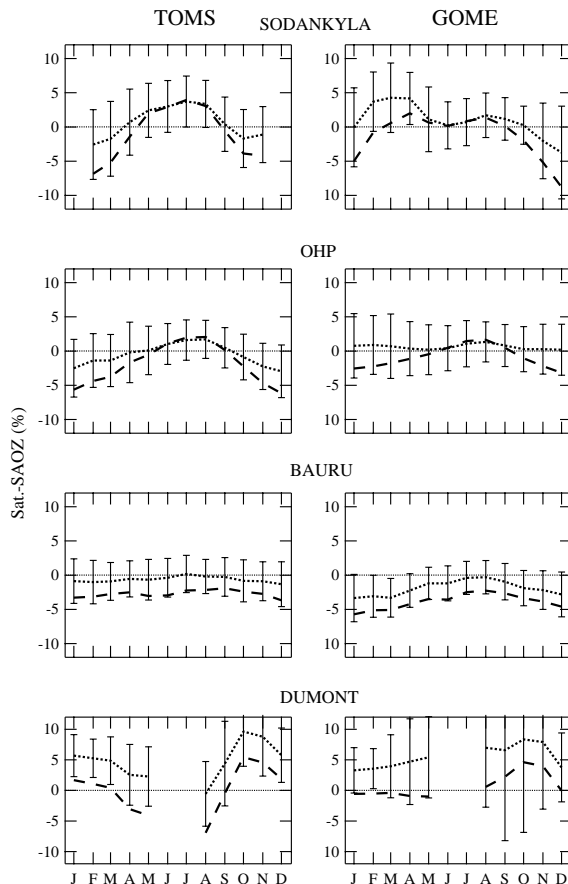


**Fig. 6.** Seasonal variation of the satellite-SAOZ relative difference (dashed: SAOZ V1, dotted: SAOZ V2). From top to bottom: Sodankyla, OHP, Bauru, and Dumont d'Urville. Left: TOMS, right: GOME-GDP4. The error bars correspond to the  $1\sigma$  deviations, which increase during the winter, particularly at high latitude.

Title Page

Abstract

Introduction

Conclusions

References

Tables

Figures

◀

▶

◀

▶

Back

Close

Full Screen / Esc

Printer-friendly Version

Interactive Discussion



**NDACC UV-visible  
total ozone  
measurements**

F. Hendrick et al.

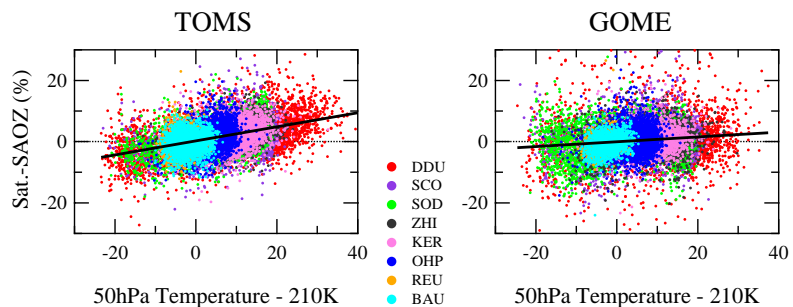


**Fig. 7.** Correlation between daily satellite-Stratospheric AOD (SAOZ) difference and ECMWF temperature at 50 hPa for the height SAOZ stations altogether. Left: TOMS, right: GOME-GDP4.

Title Page

Abstract

Introduction

Conclusions

References

Tables

Figures

◀

▶

◀

▶

Back

Close

Full Screen / Esc

Printer-friendly Version

Interactive Discussion



## NDACC UV-visible total ozone measurements

F. Hendrick et al.

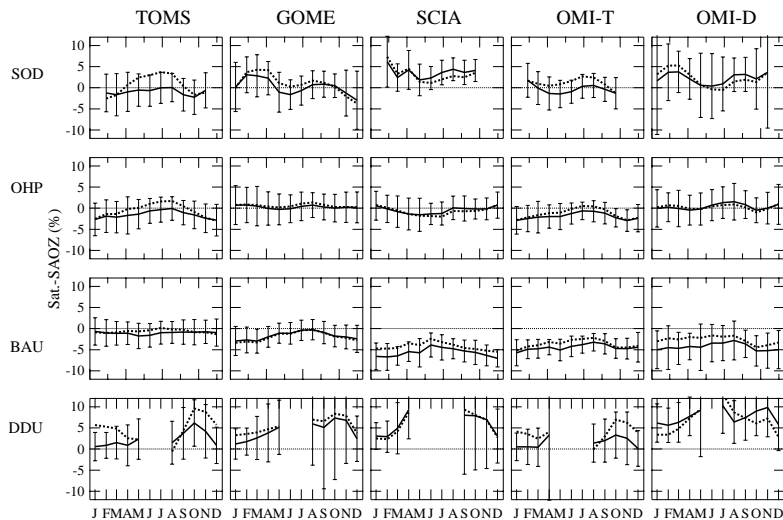


**Fig. 8.** Seasonal variations before (dotted lines) and after (solid lines) temperature correction. From top to bottom: Sodankylä, OHP, Bauru and Dumont d'Urville. From left to right: TOMS, GOME-GDP4, SCIAMACHY-TOSOMI, OMI-TOMS, and OMI-DOAS.

[Title Page](#)
[Abstract](#)
[Introduction](#)
[Conclusions](#)
[References](#)
[Tables](#)
[Figures](#)
[◀](#)
[▶](#)
[◀](#)
[▶](#)
[Back](#)
[Close](#)
[Full Screen / Esc](#)
[Printer-friendly Version](#)
[Interactive Discussion](#)


## NDACC UV-visible total ozone measurements

F. Hendrick et al.

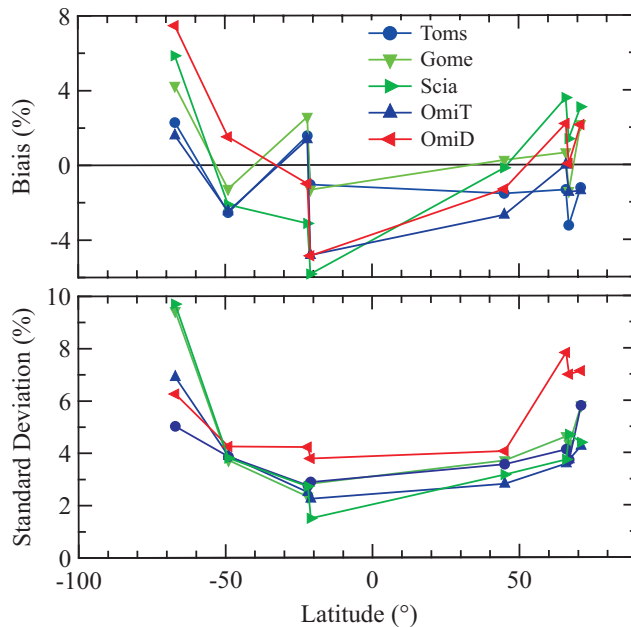


**Fig. 9.** Latitudinal variation of mean bias (top) and standard deviation (bottom) of the relative difference satellite – SAOZ V2. TOMS and OMI-TOMS (blue) show very similar results, as well as GOME-GDP4 and SCIAMACHY-TOSOMI (green). The standard deviation is larger with OMI-DOAS (red). GOME-GDP4, SCIAMACHY-TOSOMI, and OMI-DOAS display large biases in Antarctica and all systematically lower ozone at Bauru than Reunion though the two tropical stations are at the same latitude.

[Title Page](#)
[Abstract](#)
[Introduction](#)
[Conclusions](#)
[References](#)
[Tables](#)
[Figures](#)
[◀](#)
[▶](#)
[◀](#)
[▶](#)
[Back](#)
[Close](#)
[Full Screen / Esc](#)
[Printer-friendly Version](#)
[Interactive Discussion](#)


**NDACC UV-visible total ozone measurements**

F. Hendrick et al.

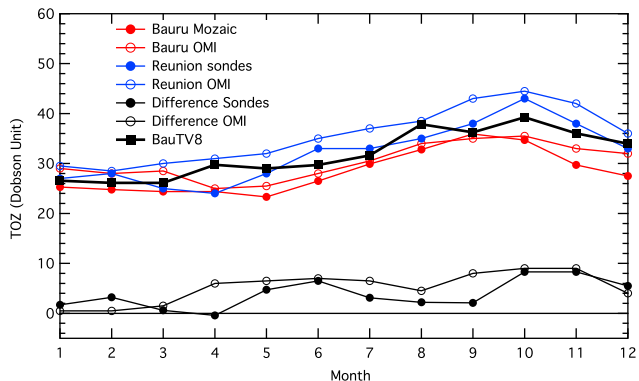


**Fig. 10.** Tropospheric ozone column over Bauru (red) and Reunion Island (blue) derived from ECC sondes or Mozaic aircraft profiles, OMI (by subtracting the MLS stratospheric ozone from the OMI total column), and TOMS V8 climatology at 20° S (thick black line). Differences Reunion-Bauru appear in black at the bottom.

Title Page

Abstract Introduction

Conclusions References

Tables Figures

◀ ▶

◀ ▶

Back Close

Full Screen / Esc

Printer-friendly Version

Interactive Discussion



**NDACC UV-visible  
total ozone  
measurements**

F. Hendrick et al.

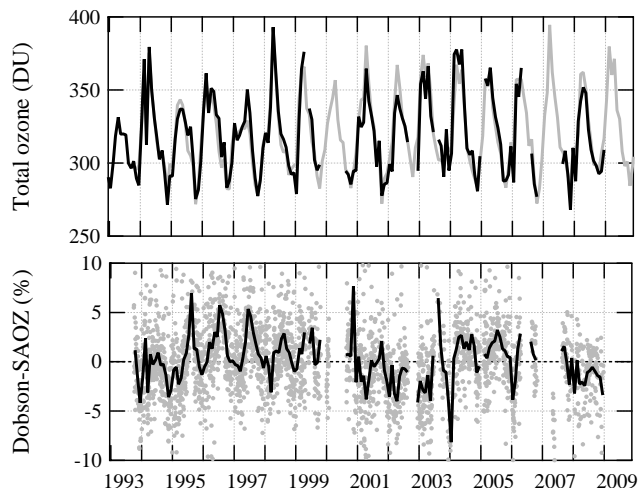


**Fig. 11.** Comparison between Dobson (black line) and SAOZ V2 (grey line) total ozone columns at OHP (upper plot). The relative difference Dobson-SAOZ V2 appears on the lower plot (grey: daily, black: monthly mean). SAOZ data in 1992–1993 are removed because of the Pinatubo eruption. The difference shows a systematic seasonal cycle, and small systematic offsets between periods of several years as well as sporadic jumps on some months. Since they do not correlate with changes in the satellite-SAOZ difference at OHP they cannot be attributed to SAOZ.

[Title Page](#)[Abstract](#)[Introduction](#)[Conclusions](#)[References](#)[Tables](#)[Figures](#)[◀](#)[▶](#)[◀](#)[▶](#)[Back](#)[Close](#)[Full Screen / Esc](#)[Printer-friendly Version](#)[Interactive Discussion](#)

**NDACC UV-visible  
total ozone  
measurements**

F. Hendrick et al.

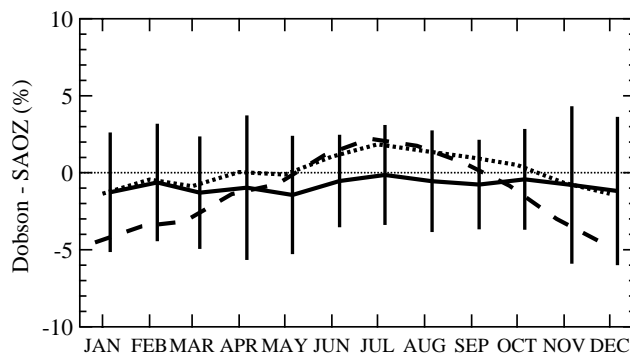


**Fig. 12.** Seasonal variation of the Dobson-SAOZ relative difference at OHP (dashed line: SAOZ V1, dotted line: SAOZ V2, solid line: Dobson corrected for temperature).

Title Page

Abstract

Introduction

Conclusions

References

Tables

Figures

◀

▶

◀

▶

Back

Close

Full Screen / Esc

Printer-friendly Version

Interactive Discussion



**NDACC UV-visible  
total ozone  
measurements**

F. Hendrick et al.

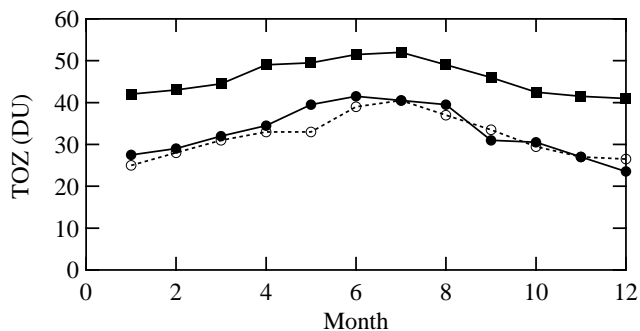


**Fig. 13.** Tropospheric ozone column at OHP derived from OMI (open circles), ECC sondes (filled circles), and TOMS V8 climatology (filled squares).

[Title Page](#)[Abstract](#)[Introduction](#)[Conclusions](#)[References](#)[Tables](#)[Figures](#)[◀](#)[▶](#)[◀](#)[▶](#)[Back](#)[Close](#)[Full Screen / Esc](#)[Printer-friendly Version](#)[Interactive Discussion](#)

**NDACC UV-visible  
total ozone  
measurements**

F. Hendrick et al.

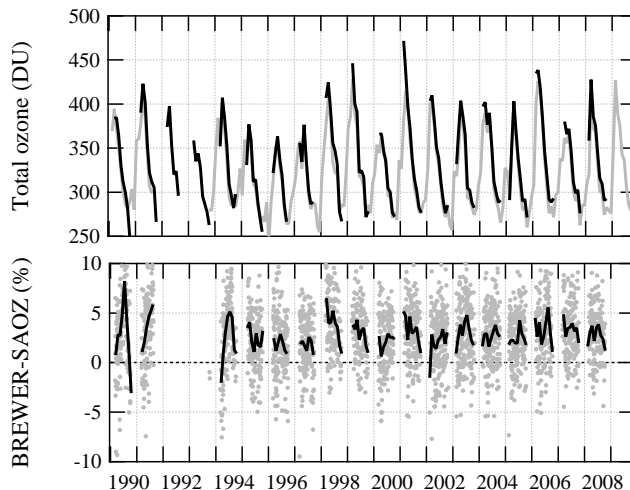


**Fig. 14.** Comparison between Brewer (black line) and SAOZ V2 (grey line) total ozone columns at Sodankyla. The relative difference Brewer-SAOZ V2 appears on the lower plot (grey: daily, black: monthly mean). SAOZ data in 1992–1993 are removed because of the Pinatubo eruption. Because of the polar night, Brewer measurements are absent during the winter. Small systematic offsets sometimes also appear, e.g., after 1997 and 2001.

Title Page

Abstract

Introduction

Conclusions

References

Tables

Figures

◀

▶

◀

▶

Back

Close

Full Screen / Esc

Printer-friendly Version

Interactive Discussion



**NDACC UV-visible  
total ozone  
measurements**

F. Hendrick et al.

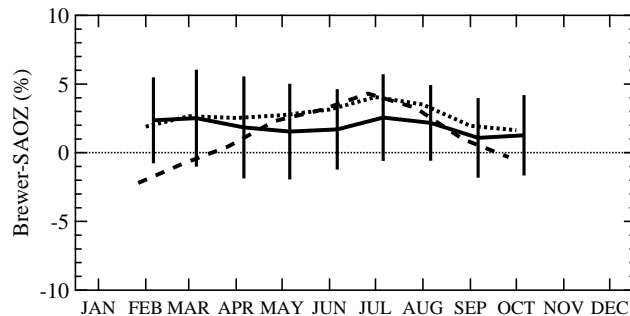


**Fig. 15.** Seasonal variation of the Brewer-SAOZ relative difference at Sodankyla (dashed line: SAOZ V1, dotted line: SAOZ V2, solid line: Brewer corrected for temperature).

[Title Page](#)[Abstract](#)[Introduction](#)[Conclusions](#)[References](#)[Tables](#)[Figures](#)[◀](#)[▶](#)[◀](#)[▶](#)[Back](#)[Close](#)[Full Screen / Esc](#)[Printer-friendly Version](#)[Interactive Discussion](#)